The changing composition of the Gulf of St. Lawrence inflow waters observed from transient tracer measurements

Lennart Gerke[1,5], Toste Tanhua[1], William A. Nesbitt[2], Samuel W. Stevens[3,4], Douglas W. R. Wallace[2]

[1]GEOMAR Helmholtz Centre for Ocean Research Kiel, Kiel, 24148, Germany
[2]Department of Oceanography, Dalhousie University, Halifax, B3H 4R2, Canada
[3]Department of Earth and Ocean Sciences, The University of British Columbia, Vancouver, V6T 1Z4, Canada
[4]Hakai Institute, Heriot Bay, British Columbia, V9W 0B7, Canada
[5][C]Worthy, LLC, Boulder, CO, 80302, USA

Correspondence to: Lennart Gerke (lennart@cworthy.org)

Abstract. The deep waters of the Gulf of St. Lawrence (GSL) have experienced a significant reduction in dissolved oxygen content during the past decades. One widely documented driver of this deoxygenation is a change in the composition of the deep inflowing water that ventilates the Gulf. This deep water is known to consist of a mix of warmer, less-oxygenated North Atlantic Central Waters (NACW) and cooler, more-oxygenated Labrador Current Waters (LCW), with prior studies inferring a shift towards increased NACW contribution. However, this compositional change has only ever been inferred indirectly from physical and biogeochemical measurements via the use of inverse methods such as water mass analysis. In this study, we present results from the first spatially-comprehensive measurements of transient tracers (SF_6 and CFC-12) in the GSL, allowing us to directly map mean age estimates and use these to infer recent changes in the composition of regional deep waters. The tracer data reveal an unexpected age distribution, with 'older' deep waters present near the Gulf's entrance, whereas 'younger' water is found further inshore, contrary to the expected estuarine circulation pattern, which transports deep water inland (increasing age along the flow path). This pattern reflects an ongoing transition toward increased NACW contribution rather than a change in the circulation itself. Our results provide direct evidence that the shift toward NACW dominated deep waters is ongoing as of 2022, contrary to earlier predictions of the complete disappearance of the younger, well-oxygenated LCW, and demonstrates the added value of transient tracers for constraining ventilation and water mass evolution in the GSL.

1 Introduction

Ocean ventilation is a physical process that involves the dynamic exchange of properties like heat and dissolved gases, including oxygen, between the atmosphere and the ocean's interior (Azetsu-Scott et al., 2005; Fine, 2011; Talley et al., 2016). It describes the transport of surface waters to the interior of the ocean, where the age of the water refers to the time since a water parcel was last in contact with the atmosphere. This process is, for example, important in distributing oxygen to deeper ocean layers and in shaping long-term properties of water masses in the interior, in contrast to the rapidly changing surface water layers. Ventilation studies often rely on measurements of transient tracers, such as sulfur hexafluoride (SF_6) and chlorofluorocarbon-12 (CFC-12), anthropogenic gases which are inert once dissolved in seawater and whose input can be characterized by known variations of concentrations in the atmosphere (e.g. Khatiwala et al., 2001; Stöven et al., 2015). SF_6 and CFC-12 are particularly useful and widely used in oceanography because their atmospheric history is well constrained and by measuring their concentration in seawater and comparing them to atmospheric input functions, it is possible to estimate how long water has been isolated from the atmosphere, i.e., its 'ventilation age'. CFC-12 with longer atmospheric history, is effective for tracing somewhat older water, while SF_6 is more sensitive to recently ventilated waters. After the surface water is shielded from the atmosphere due to transport into the interior, the abiotic transient tracer concentrations are only affected by interior mixing processes since these compounds are stable in seawater during most conditions. By combining measurements of both tracers enables to resolve water mass formation, mixing, and circulation patterns, which are key to understanding distribution of biogeochemical properties, such as oxygen. Ventilation has been well-studied in certain regions

of the world's oceans using transient tracers, but remains largely unexplored in others, particularly in marginal seas such as the Gulf of St. Lawrence (GSL).

Recently, the GSL region has garnered attention due to a significant decline in dissolved oxygen (DO) concentrations within the deep layer (e.g. Blais et al., 2024; Genovesi et al., 2011; Gilbert et al., 2005; Thibodeau et al., 2006), leaving a growing area persistently hypoxic (DO < 62.5 μmol L^{-1} (micromoles of O_2 molecules present in 1 L of seawater)) (Jutras et al., 2023b). Among other property changes, it was reported that the annual average of DO at 300 m depth in the Estuary of the Gulf dropped to 37 μmol L^{-1} in 2023 (12 % saturation) (Blais et al., 2024). This phenomenon has been observed increasingly in coastal zones worldwide during the past few decades (Diaz and Rosenberg, 2008; Gilbert et al., 2005), for example due to benthic respiration (Lehmann et al., 2009), upwelling of low-oxygen waters (Grantham et al., 2004) and long residence times in ocean channels enhancing hypoxia (Fennel and Testa, 2019). In the well-studied region at the head of the Lower St. Lawrence Estuary (LSLE), deep layer DO values decreased from 130 μmol L^{-1} to 60 μmol L^{-1} between 1930 and 1984 where they then remained stable until about 2019. In 2020, concentrations rapidly decreased to an annual minimum of 35 μmol L^{-1} (Jutras et al., 2023b), with further, slight decrease observed in 2022 and 2023 by Blais et al. (2023, 2024), down to 34 μmol L^{-1}. Based on extensive measurements in this region, the hypoxic zone was first documented in the LSLE (Gilbert et al., 2005), with two-thirds of the decrease in DO since 1930 being estimated to be caused by a change in the composition of the deep water masses entering the GSL from the North Atlantic, and the other third being due to eutrophication (Gilbert et al., 2005; Mucci et al., 2011). The oceanic inflow supplies the deep-water layers of the GSL with oxygen, and is known to consist of a mix of well-oxygenated Labrador Current Water (LCW) and less-oxygenated North Atlantic Central Water (NACW). Several studies, such as Gilbert et al. (2005) and Jutras et al. (2020), identified a shift in the composition of the deep-water inflow toward a larger fraction of NACW using physical and chemical parameters, as well as inverse methods such as water mass analysis.

Previous estimates of LCW and NACW fractions at Cabot Strait have shown considerable temporal variability. For instance, Gilbert et al. (2005) reported a shift from 72 % LCW and 28 % NACW in 1930 to 53 % LCW and 47 % NACW over the period of 1980 to 2003, consistent with earlier estimates from Bugden (1988) when using their definition of LCW, which incorporates temperature, salinity and oxygen characteristics. More recently studies have continued to document this evolution. Jutras et al. (2020) reported LCW fractions of less than 10 % on the $\sigma_\Theta = 27.3$ kg/m^3 isopycnal in 2017, and around 50 % at $\sigma_\Theta = 27.5$ kg/m^3, indicating a stronger LCW influence at greater depths. In Jutras et al. (2023b), LCW fractions at Cabot Strait were reported as 0 % in 2021, with only small LCW influence at intermediate depths (~250 m) within the Laurentian Channel from a longitude of Anticosti Island to the LSLE. Together these studies suggest a progressive but variable transition toward increased NACW contribution over the past decades.

The study by Jutras et al. (2020) utilized the extended optimum multiparameter analysis (eOMP), which relies typically on conservative and quasi-conservative hydrographic properties such as temperature, salinity, nutrients, and/or oxygen. This study incorporates transient tracer measurements (SF_6 and CFC-12) which provide additional insight into the ventilation timescales (mean age) of subsurface water parcels and enhances the analysis of water composition through the use of parameters that carry additional information about temporal changes and mixing processes.

This study first focusses on the independent use of transient tracers to estimate ventilation timescales within the deep water of the GSL via a transit time distribution (TTD) analysis. These tracer-derived mean ages are then integrated into a water mass analysis to provide a detailed assessment of the water mass composition. This demonstrates that inclusion of tracer measurements improves the resolution of compositional shifts in the GSL and highlights that incorporating transient tracers is valuable to complement more traditional hydrographic data in methods such as eOMP.

2 Hydrography

The St. Lawrence Estuary and Gulf is one of the largest semi-enclosed estuaries in the world and consists of three components: the Upper Estuary ranging from Ile d'Orleans to Tadoussac, the LSLE spanning from Tadoussac to Pointe-des-Monts, and finally the GSL. The GSL is a large marginal sea (approximate area of 240 000 km^2) located at the east coast of North America, and is connected to the Atlantic Ocean through Cabot Strait between Nova Scotia and Newfoundland in the southeast, and to the Newfoundland and Labrador Shelf via the Strait of Belle Isle in the northeast (see Figure 1). Due to its depth, Cabot Strait is the main entry point for North Atlantic water, which enters as a deep inflow (Koutitonsky and Budgen, 1991).

The GSL includes itself three channels (slightly darker blue areas in Figure 1), one south of Anticosti Island (Laurentian Channel), connecting the GSL to the Atlantic Ocean, one north of the Island (Anticosti Channel) and one channel towards the Strait of Belle Isle (Esquiman Channel), all bordering extensive shelf areas.

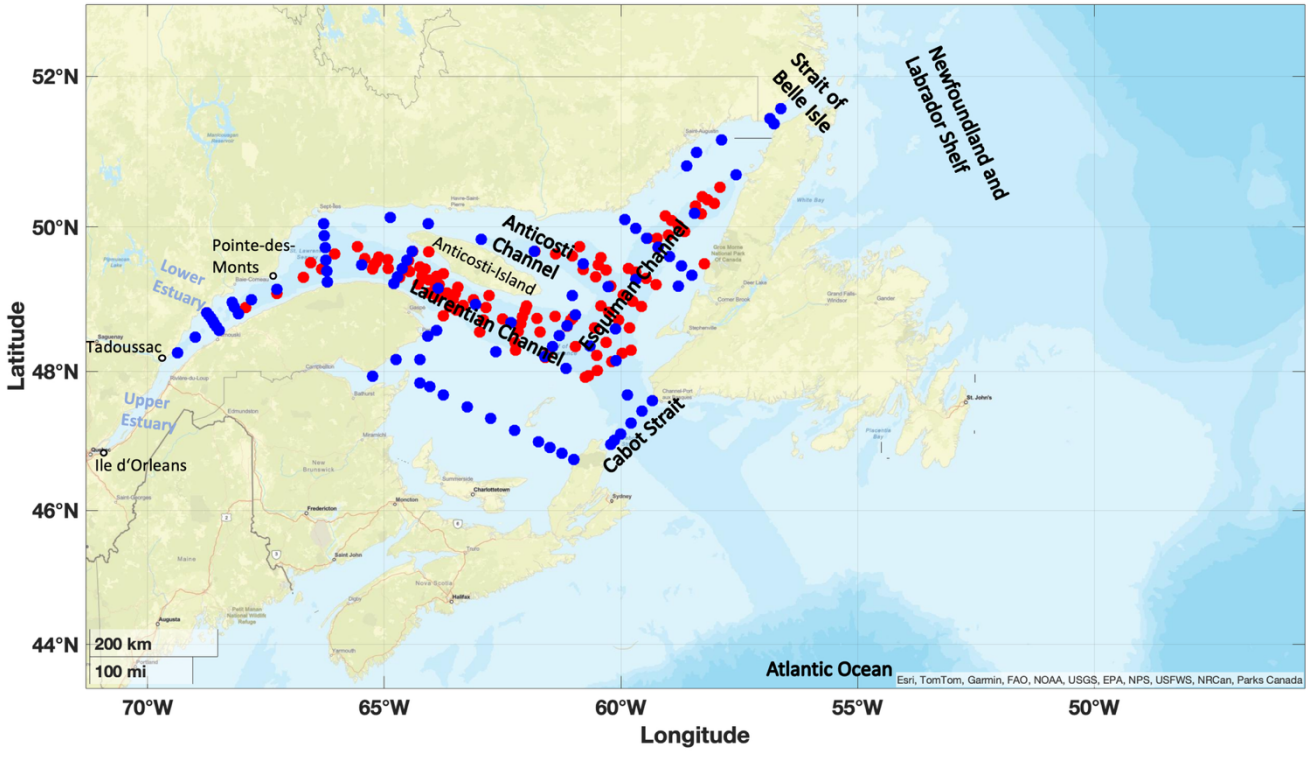

Figure 1: The Gulf of St. Lawrence, with its main Channels and Straits identified, together with the Lower and Upper Estuary. Sampling stations from the expeditions in June 2022 (TReX 2 – red dots) and November 2022 (DFO's AZMP survey/TReX 4 – blue dots) are displayed.

The current that feeds deep water into the Gulf of St. Lawrence from the Atlantic Ocean carries two constituents, LCW and NACW, which enter at depths exceeding 200 m through Cabot Strait, forming the relatively warm and saline deep water of the GSL (θ = 1 °C to > 7 °C and S_p = 32.5 to 35) (Galbraith et al., 2024; Lauzier and Trites, 1958; McLellan, 1957).

In addition to the deep water entering the Gulf through Cabot Strait, the water column structure consists of an intermediate layer and a surface layer. The cold (< 1 °C) and saline intermediate layer (CIL – Cold Intermediate Layer), is mainly formed locally during winter due to interior water mixing when cooling and formation of sea ice increases the density of the surface water (Galbraith, 2006). A small fraction of the CIL also originates from the inflow of cold water from the Labrador Shelf through the Strait of Belle Isle and an even smaller contribution originates through Cabot Strait at intermediate depths (Galbraith, 2006; Shaw and Galbraith, 2023). The intermediate water layer in the LSLE and Upper St. Lawrence Estuary consists of less salty water, which is renewed by saltier CIL water moving inland from the Gulf in spring (Galbraith, 2006). The relatively warm in summer (> 1 °C) and low salinity surface water flows mainly seaward, thereby transporting the continental runoff freshwater from the Estuary, and water from the north shore rivers towards the Atlantic Ocean (Galbraith, 2006; Gilbert and Pettigrew, 1997). This outflow leaves the Gulf through the southern edge of Cabot Strait, as the inflow mainly occurs around the northern boundary of the strait (Galbraith et al., 2024).

Using ocean models, the transit times of the deep water within the Laurentian Channel transported from Cabot Strait until the head of the channel range from 2 to 7 years, depending on the depth (Saucier et al., 2003). For instance, Gilbert (2004) estimated water at depths of 250 m to flow inland from the Atlantic Ocean with a speed of 1 cm/s, reaching Cabot Strait after 1 year and the Estuary after 3.5 years, i.e. a transit time of 2.5 years from Cabot Strait to the Estuary. Recently, Rousseau et al. (2025) provided and integrated estimates for the transit time of the entire deep water column (>225 m), being 3.2 ± 0.7 years from Cabot Strait to the head of the Laurentian Channel. The transit time was analyzed in detail by Stevens et al. (2024) including measurements of a deliberately released tracer experiment (TReX), that estimated the time for the first water parcels to reach the head of the Gulf to be 1.7 years from Cabot Strait with the bulk of the water arriving after around 4.7 years (in approximate agreement with the earlier estimates of Bugden (1988)). This estimate represents waters centred around the density surface of σ_Θ = 27.26 kg/m^3, representing the water layer from ≈ 250 – 310 m within the Laurentian Channel.

As the transient tracer measurements that we present in this study were collected in tandem with data collected for the TReX tracer experiment, as detailed in Stevens et al. (2024), we use the advection timescales presented in that study to inform our analyses. Furthermore, we also choose the same density surface of σ_Θ = 27.26 kg/m^3 to represent the core of the deep water inflow.

3 Data and Methods

3.1 Surveys

The data analyzed in this study was obtained during two field campaigns, one in June 2022 (TReX 2) and one in November 2022 (DFO's AZMP Survey/TReX 4), both carried out on the Canadian research vessel '*R/V Coriolis II'*. The primary objective of the TReX 2 field campaign was to track the deliberately-released tracer trifluoromethyl sulfur pentafluoride (SF_5CF_3), which was release in October of 2021 on the density surface of $\sigma_\Theta = 27.26$ kg/m^3 within the Laurentian Channel, as part of the TReX experiment aiming at monitoring the transport pathways for the deep water in the GSL. Since the released tracer and the transient tracers focused on in this study, CFC-12 and SF_6, were measured simultaneously, sampling was concentrated primarily on this density layer, resulting in an uneven depth-distribution of transient tracer observations.

The June cruise was supported by the Marine Environmental Observation, Prediction and Response Network (MEOPAR) and Réseau Québec Maritime (RQM), whereas the November cruise was conducted by the Department of Fisheries and Oceans, Canada (DFO) as part of the Atlantic Zone Monitoring Program (AZMP). The AZMP leads regular surveys along fixed sections since 1999 to monitor physical and biological processes in the St. Lawrence Seaway and the coastal shelf of Eastern Canada, around Nova Scotia and Newfoundland.

Both cruises sampled sections in the Laurentian Channel, the Anticosti Channel, the Esquiman Channel, and the later cruise included sampled stations at Cabot Strait (see Figure 1) (Blais et al., 2023).

3.2 Observation parameters

The observed tracer concentrations of CFC-12 and SF_6, measured simultaneously throughout both 2022 cruises covering the entire GSL and LSLE, were used to estimate water mass mean ages. By comparing the measured concentrations in seawater to the known time-varying atmospheric concentrations of these tracers, it is possible to estimate the time elapsed since a water parcel was last in contact with the atmosphere, providing a robust measure of ventilation and water mass age. Assuming a saturation state that reflects equilibrium between surface water and atmosphere, knowing the solubility, and the tracers' atmospheric concentration as a function of time (Bullister et al., 2002; Bullister and Warner, 2017; Warner and Weiss, 1985), it is possible to reconstruct the historical input functions of each tracer at the sea surface. Since the concentration of SF_6 continues to increase in the atmosphere, it can be used to estimate ventilation over approximately the last 40 years. CFC-12, on the other hand, is more appropriate for slightly older water masses, as its production started around 1940, but its atmospheric concentration has decreased since 2002 (see Figure S1). Nevertheless, measurements of more than one tracer are needed to provide information on ventilation patterns and determine, for example, if this process is more advectively or diffusively dominated (e.g. Stöven et al., 2015).

Both tracers were measured concurrently on board of the research vessel with a gas chromatographic – electron capture detector system attached to a custom purge and trap unit (GC-ECD/PT5) (Bullister et al., 2002; Gerke et al., 2024; Tanhua et al., 2004,

2005b). The system has a detection limit of approximately 0.03 fmol/kg and 0.02 pmol/kg for SF_6 and CFC-12, respectively (Stöven et al., 2015), and all measured concentrations during the two surveys showed values well above the system's detection limits. For details on the GC-ECD/PT5 system and data calibrations, see Appendix A.

The TTD (transit time distribution) method is a well-established and widely used concept to represent ventilation and allows calculation of various characteristics of the age distribution for a parcel of water in the ocean, including its mean age (e.g. Hall and Plumb, 1994; Shao et al., 2016; Trossman et al., 2012). As described in detail in Appendix B, we constrained the most suitable TTD for this region using our measured tracers' concentrations in combination with a time dependent saturation estimated by Raimondi et al. (2021) and a Δ/Γ-ratio (width of the distribution to mean age ratio) of 1.2. As only relatively young water is present within the Gulf, we calculated the final mean ages using the measured SF_6 concentrations in combination with the TTD which was determined through the use of both tracers. Note that in this study the term "age" refers to the time elapsed since a water parcel was last in contact with the atmosphere, i.e. since it was ventilated, not the time since it entered the GSL.

We use potential temperature (θ) and practical salinity (Sp) to infer the composition of the Gulf inflow waters, and the transient tracers to analyze the ventilation timescale of these waters. The θ and S_p data was obtained via CTD sensors during both surveys (e.g. Blais et al., 2023). In addition, both cruises included oxygen probe measurements (SVE-43 DO probe) calibrated by Winkler titration from collected water samples (Hansen, 1999).

Uncertainties in the mean age values arise from various factors, including uncertainties in the tracer measurements ($\approx$ 2 %), uncertainties in constraining the TTD, and most significantly from the input functions used (i.e. atmospheric concentration and saturation assumption). Considering all these factors, an uncertainty of 10 % is applied to the calculated mean ages, represented by error bars. See Appendix C for details on each of the uncertainty factors.

To provide context on water masses before entering the GSL, we used data from the GLODAPv2.2022 (Global Ocean Data Analysis Project version 2) data product (Lauvset and et al., 2022), which compiles globally quality-controlled measurements of transient tracers and other oceanographic parameters from cruises worldwide. GLODAP covers measurements in the broader North Atlantic and allows characterization of water masses, such as LCW and NACW, before they enter the GSL. We focused specifically on data collected after 2010 in the region near the mouth of the Laurentian Channel, where the deep water enters, while still representing LCW and NACW as distinct unmixed water masses (see Figure 4b). Mean ages were primarily computed from CFC-12 measurements due to higher abundance of this tracer in those regions around the mouth of the Laurentian Channel. The same saturation and Δ/Γ-ratio, as determined earlier were considered for the calculation, being consistent with conditions in LCW and NACW, as water residence times before entering the Gulf are relatively short. However, because only CFC-12 was measured in these regions, it was not possible to derive local Δ/Γ-ratio directly, which introduces some uncertainty to the age estimates.

3.3 Water mass analysis

3.3.1 Linear fraction model

To obtain detailed information on the water mass composition of the deep water, we use a linear fraction model including the three parameters, mean age (Γ), θ and *S*p (see Equations 1- 4) and solve it for a least square solution of fractions.

$$\Gamma_{obs} = f_{LCW} * \Gamma_{LCW} + f_{NACW} * \Gamma_{NACW} \quad (1)$$

$$\theta_{obs} = f_{LCW} * \theta_{LCW} + f_{NACW} * \theta_{NACW} \quad (2)$$

$$Sp_{obs} = f_{LCW} * Sp_{LCW} + f_{NACW} * Sp_{NACW} \quad (3)$$

$$1 = f_{LCW} + f_{NACW} \quad (4)$$

Here, the observed values represent the measured parameters within the GSL (Γ_{obs}; θ_{obs}; Sp_{obs}) during 2022, f_{LCW} and f_{NACW} display the individual fractions of the two mixing water masses and Γ_{LCW}, Γ_{NACW}, θ_{LCW}, θ_{NACW}, Sp_{LCW} and Sp_{NACW} indicate the endmembers of the two water masses before mixing. The endmembers for temperature and salinity are set to be the mean of the θ and *S*p range of LCW and NACW, respectively, as presented in Jutras et al. (2020). For the mean age endmembers, we collated tracer data measured outside the GSL since 2010 in the respective temperature, salinity and density ranges, representing the LCW and NACW and computed the endmembers for the water mass analysis from the mean of the calculated mean ages within the respective water mass (see Table 1). All parameters are considered quasi-conservative (i.e., not affected by biogeochemical processes) given the short transit time from immediately outside the GSL to the Laurentian Channel, making the use of mean age endmembers plausible (Tanhua et al., 2005a).

Table 1: Endmembers of θ, *S*p and Γ used for the water mass analysis alongside each water mass fraction range. Note that the mean age endmembers are represented by the mean of all computed values, not representing the middle of the range.

Variables	NACW range	LCW range	NACW endmember	LCW endmember
Θ [°C]	4.4 – 8	-0.7 – 3.2	6.2 ± 1.04	1.25 ± 1.13
*S*p [psu]	35 – 35.2	33.4 – 35	35.1 ± 0.06	34.2 ± 0.46
Γ [years]	49 – 105	7 – 19	86.5 ± 1.67	12.5 ± 0.23

This linear approach bears uncertainties, such as the selection of the individual endmembers, uncertainty in the parameter observations used for the fraction calculation, and structural model assumptions, including the equal weighting of parameters in a simple least square solution.

To address these uncertainties, we estimated the ambiguity in the selection of the mean age endmembers as the standard error of the mean (SEM) from the individual measurements within each water mass in the Atlantic Ocean. This resulted in endmember uncertainties of 1.67 years for NACW and 0.23 years for LCW. For temperature and salinity endmembers, uncertainties were approximated using uniform distributions across the reported parameter ranges, resulting in uncertainties of 1.04 °C and 1.13 °C for NACW and LCW temperatures, respectively, and 0.06 and 0.46 psu for NACW and LCW salinities. The mean age observations within the Gulf, included in the fraction analysis, were assigned a relative uncertainty of 10 %, as previously specified, while errors in temperature and salinity observations were considered negligible. An additional 20 % relative uncertainty was introduced to account for structural assumptions in the simple linear mixing model. All uncertainties were jointly propagated using a Monte Carlo approach (N = 10,000) (JCGM, 2008), yielding in an overall LCW fraction uncertainty of approximately 21 %. A detailed uncertainty budget analysis is provided in Appendix D.

Despite these uncertainties, this method offers a comparison to the ventilation timescales derived from the transient tracer measurements and provides additional insights into water mass composition by more effectively capturing temporal changes and mixing processes in comparison to the other methods solely relying on hydrographic parameters.

3.3.2 2-IG-TTD approach

As this study utilized measurements of multiple tracers, we also applied a two-inverse Gaussian transit time distribution (2-IG-TTD) approach to analyze the water mass composition. This method accounts for the presence of two water masses with distinct age characteristics mixing within the same density surface (For details, see Stöven and Tanhua, 2014). In this framework, the system is represented by a linear combination of two IG distributions, characterized by separate mean ages (Γ1, Γ2) and widths (Δ1, Δ2), with a mixing fraction α controlling the relative contribution of each component.

$$c(t,r) = \int_0^\infty c_0(t-t')e^{-\lambda t'} * [\alpha * G(\Gamma_1, \Delta_1, t', r) + (1-\alpha) * G(\Gamma_2, \Delta_2, t', r)]\, dt' \quad (5)$$

The total mean age of the resulting water parcel is then calculated as:

$$\Gamma = \alpha * \Gamma_1 + (1-\alpha) * \Gamma_2 \quad (6)$$

Considering the average mean age endmembers of the NACW and LCW, as described above and having computed mean ages within the GSL, we can calculate the mixing fraction α, representing the water mass fraction.

3.4 Deep water time proxy at Cabot Strait

A proxy time series at Cabot Strait was constructed to better resolve temporal changes in mean age and water mass composition and potentially related water mass properties, such as oxygen. This approach provides a clearer view of long-term trends compared to basin-wide observations based on single-year measurements. Rather than sampling repeatedly at a fixed station, measurements from 2022 along the Laurentian Channel were combined with the estimated deep water transit time from Stevens et al. (2024) to infer when each water parcel would have passed Cabot Strait. For each sample, the distance to a fixed reference location within Cabot Strait (47.2 °N; 59.7 °W) was used together with an average transit speed of 0.5 cm/s to assign an equivalent passage date through Cabot Strait. This allowed construction of a time series representative of inflowing water over multiple years. In addition to the time series adjustment, the DO concentrations were corrected for consumption over time using the estimated oxygen utilization rate (OUR) within the Laurentian Channel, of 21.1 μmol/kg per year (Nesbitt et al., 2025). The resulting adjusted oxygen values are reported in the Supporting Information (see Figure S2)

4 Results

4.1 Water mass distribution

During both cruises, all three water layers of the GSL, the warm and fresh surface, the cold intermediate and deep water, defined as in Galbraith et al. (2024), were clearly present (see Figure 2).

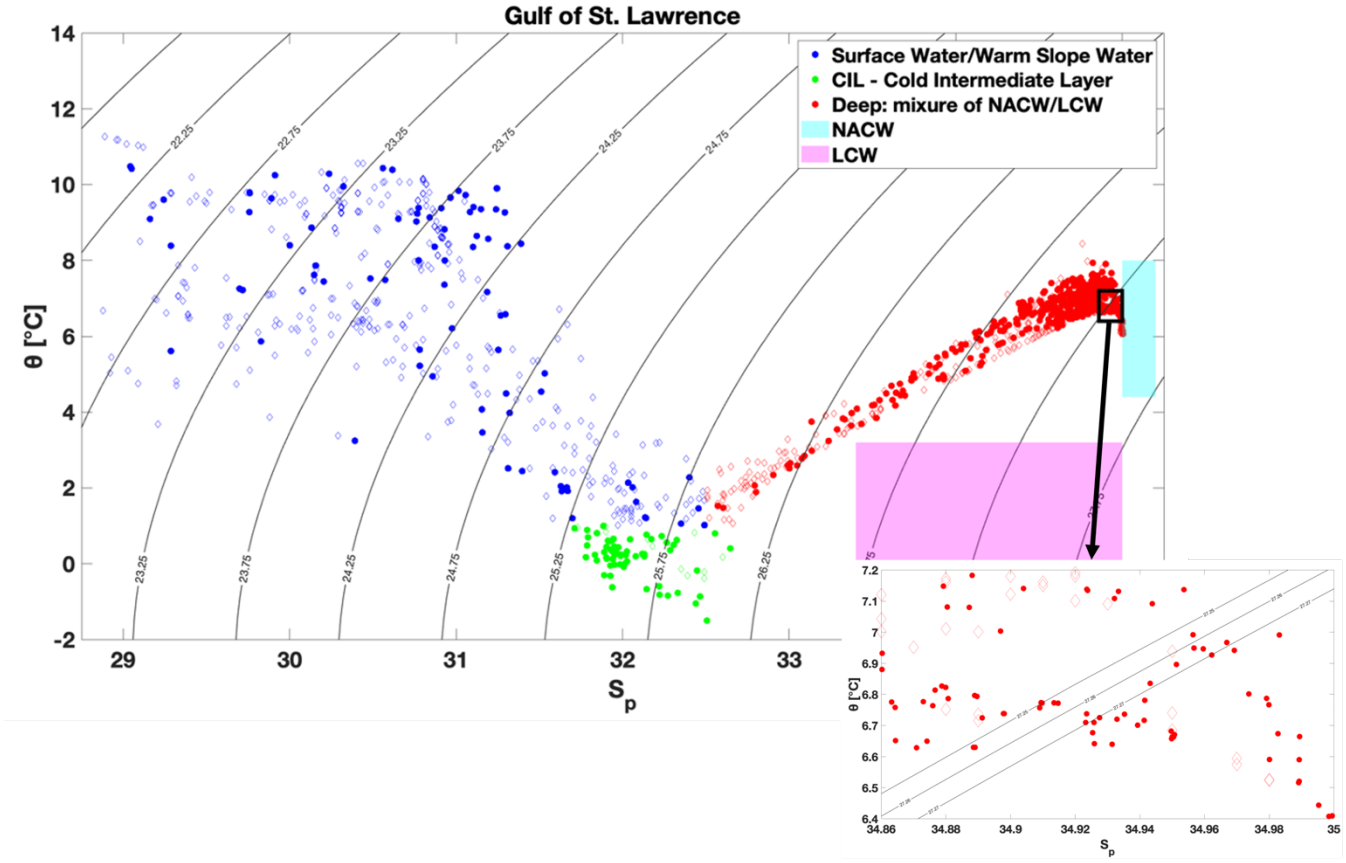

Figure 2: Potential Temperature (θ) vs Practical Salinity (S_p) plot from the bottle data of the two cruises in 2022, showing the three main layers of the GSL, as indicated by different colors with density lines of σ_Θ (TReX 2 – dots; DFO's AZMP survey/TReX 4 – diamonds). The pink and the cyan areas represent the θ vs S_p ranges of LCW and NACW, as defined in Jutras et al. (2020)**. In addition, a zoomed in area around the density of $\sigma_\Theta = 27.26$ kg/m^3 is shown, with density lines at 27.25, 27.26 and 27.27.**

The temperature and salinity structure throughout the water column was similar during both cruises (see Figure 2 – dots and diamonds) with the deep temperature maximum (8 °C) present at depths between 200 and 300 m in the Laurentian Channel. In recent years, the temperature at these depths has increased from an average of 5.2 °C in 2009 to 7 °C in 2022, with the warmest water being observed near Cabot Strait, where temperatures exceeding 7 °C were measured as early as 2012 (Galbraith et al., 2024). As our study and the sampling strategy of TReX 2 focus on the region's deep layer, we concentrate on properties in the core of the deep-water layer on the $\sigma_\Theta = 27.26$ kg/m^3 isopycnal (250 – 310 m) (see Figure 3). Note that on this isopycnal, temperatures vary from approximately 6.4 °C to 7.5 °C and salinity varies from 34.7 to 34.95 (see Figure 3c – 3f).

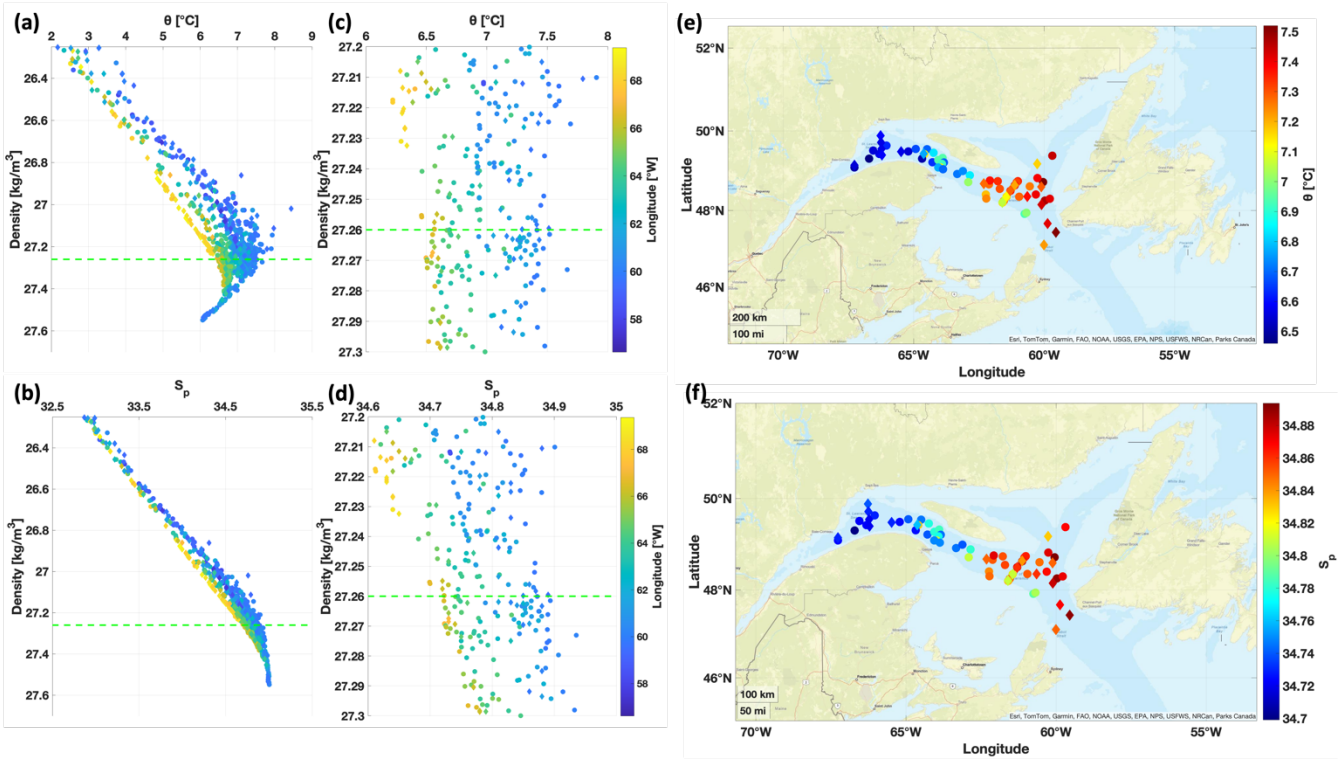

Figure 3: Potential Temperature (a) and Practical Salinity (b) measured within the deep-water layer in the GSL (density > 26.25 kg/m^3), with the colorbar representing the longitude. Figures c and d represent a zoomed in area around the σ_Θ = 27.26 kg/m^3 isopycnal (green dotted line) and plots e and f show these measurements plotted on a map of the GSL against longitude and latitude. All the data presented here was collected during the two surveys in 2022, with the dots represent the measurements from the earlier survey (TReX 2) and the diamonds the measurements from the later cruise (DFO's AZMP survey/TReX 4).

Colder and less saline waters were observed to the west of the region within the entire deep-water layer (see Figure 3a & 3b). Focusing on the σ_Θ=27.26 kg/m^3 isopycnal (see Figure 3c – 3f) this is also evident, alongside a sudden discontinuity in both variables at approx. 63 °W (eastern tip of Anticosti Island).

4.2 Age distribution around the σ_Θ = 27.26 kg/m^3 isopycnal

When examining the mean age of water from tracer data collected since 2010 in the Atlantic region outside the GSL, focusing on a density of σ_Θ = 27.26 kg/m^3 (see Figure 4b), we observe the oldest water (70 – 105 years) to be located south/southwest of Cabot Strait, over the Scotian shelf and areas southeast of it, with considerably younger water located to the northeast (5 – 20 years), near the Newfoundland Shelf and Flemish Cap. Although these mean ages exceed the direct atmospheric history of CFC-12 (tracer age), the values are plausible because the mean age is derived from the IG-TTD, which reflects a full distribution of transit times, including its older tail (see also Guo et al. (2025), who showed that water masses with ideal ages

295 up to 200 years can still be well represented by CFC-12 based IG-TTD analysis). This reflects the distribution of more recently ventilated LCW dominant in the northeast of the region and the older NACW in the south and southwest. The influence of the younger LCW is visible near the entrance to the Gulf, where there is a reduction in age of the northward-flowing NACW. At the mouth of the Laurentian Channel, the age of the deep waters is around 40 – 50 years.

The observations of the GSL deep water shows that the water close to Cabot Strait is older compared to waters located closer
300 to the Lower Estuary (see Figure 4a). This age distribution is consistent with distributions of temperature and salinity (see Figure 3), where 'younger' waters have higher LCW composition (colder and less salty, more oxygen) and 'older' waters have higher NACW composition (warmer and saline, less oxygen). Consistent with the temperature and salinity spatial variability, deep layer mean age shows an abrupt 5 – 10 year shift towards younger waters at approximately 63 °W (i.e., the southeastern tip of Anticosti Island), as indicated by the contrast between blue (west of 63 °W) and red (east of 63 °W) sampling stations
305 in Figure 4c. On the $\sigma_\Theta = 27.26$ kg/m^3 isopycnal, we see a shift in age from around 45 years to 35 years (see Figure 4d). Apart from this sudden shift, the mean age generally increases gradually between the LSLE and Cabot Strait. On the studied isopycnal, mean age values are largest at Cabot Strait (60 years), with younger waters (40 – 50 years) present in the eastern part of the Laurentian Channel between 61 °W and 63 °W and the youngest waters located to the west of 63 °W (30 – 40 years; see Figure 4a).

310 Even though we focused sampling on the $\sigma_\Theta = 27.26$ kg/m^3 isopycnal, samples collected on other isopycnals in the deep layer show comparable results, with younger water observed further inland relative to measurements taken closer to Cabot Strait (see Figure 4c). Additionally, in the intermediate layer, at densities between $\sigma_\Theta = 25.25 – 26.25$ kg/m^3, similar trends were observed in age and tracer concatenations despite the sparse data coverage.

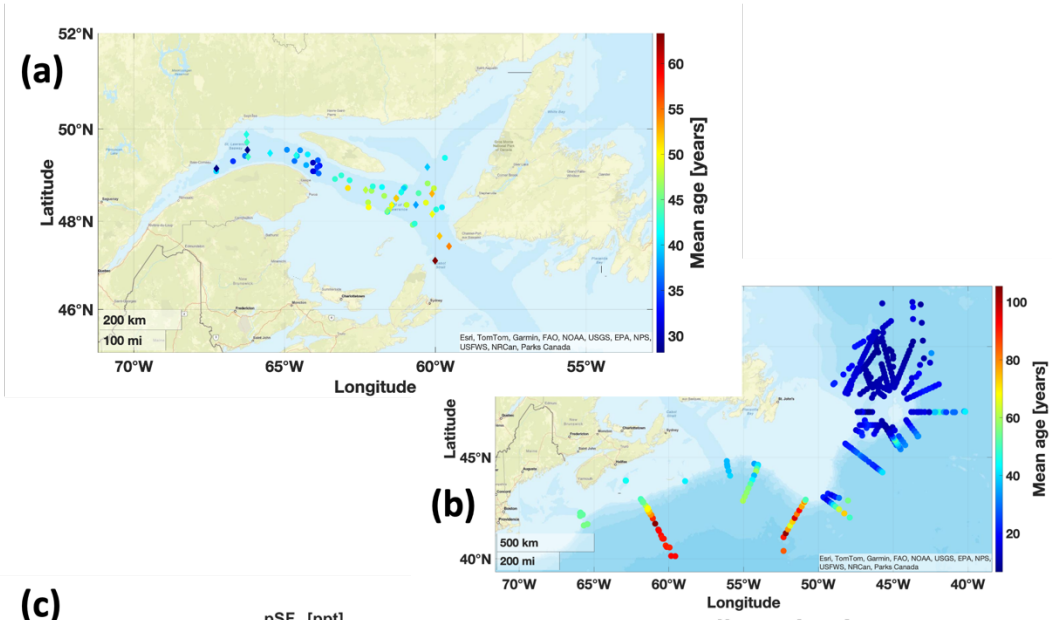
(a)
52°N
50°N
48°N
46°N
Latitude
70°W
65°W
60°W
55°W
Longitude
200 km
100 mi
Esri, TomTom, Garmin, FAO, NOAA, USGS, EPA, NPS, USFWS, NRCan, Parks Canada
Mean age [years]
60
55
50
45
40
35
30
(b)
45°N
40°N
Latitude
70°W
65°W
60°W
55°W
50°W
45°W
40°W
Longitude
500 km
200 mi
Esri, TomTom, Garmin, FAO, NOAA, USGS, EPA, NPS, USFWS, NRCan, Parks Canada
Mean age [years]
100
80
60
40
20

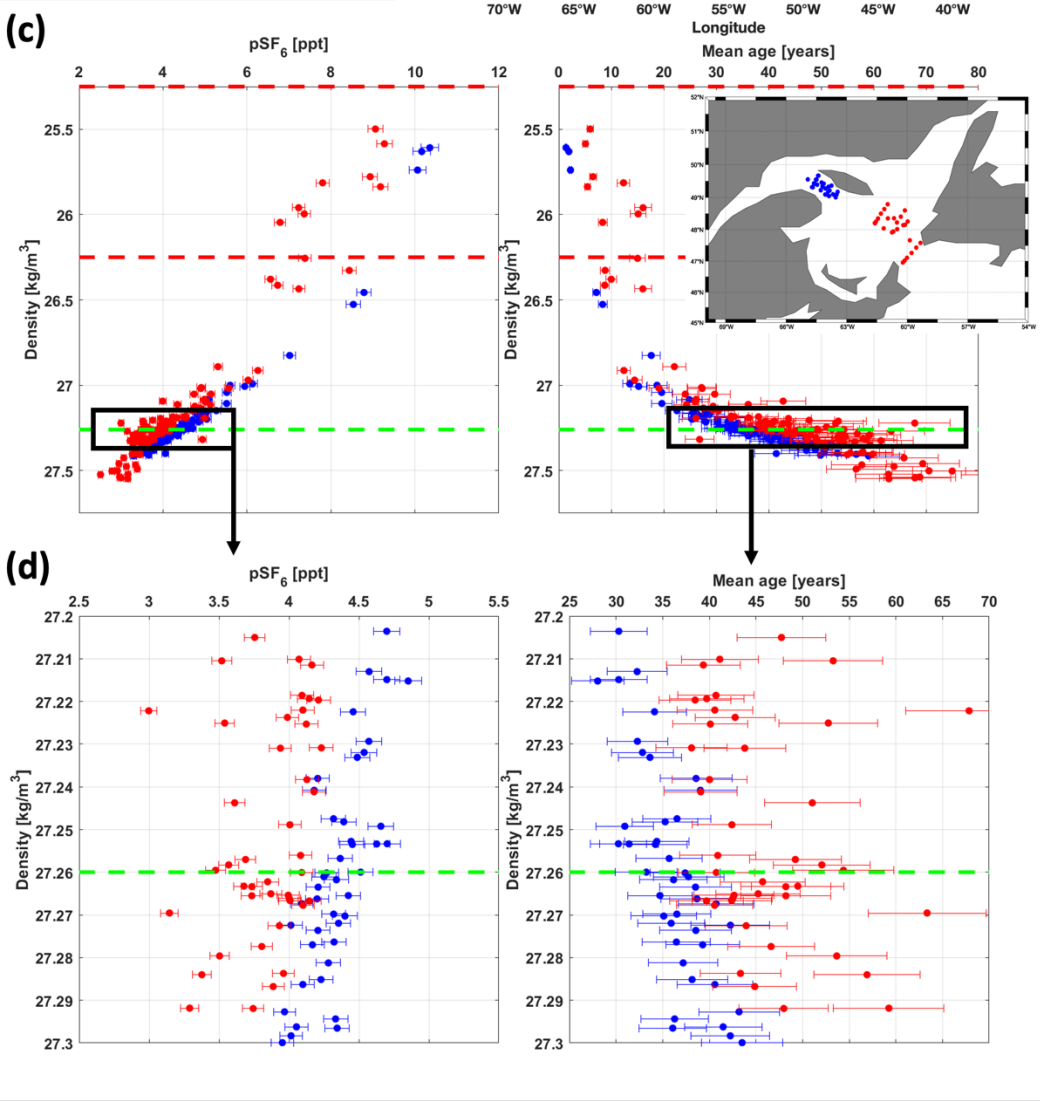
(c)
pSF6 [ppt]
2
4
6
8
10
12
Density [kg/m3]
25.5
26
26.5
27
27.5
Mean age [years]
0
10
20
30
40
50
60
70
80
(d)
pSF6 [ppt]
2.5
3
3.5
4
4.5
5
5.5
Density [kg/m3]
27.2
27.21
27.22
27.23
27.24
27.25
27.26
27.27
27.28
27.29
27.3
Mean age [years]
25
30
35
40
45
50
55
60
65
70

315

Figure 4: a) Mean age on the $\sigma_\Theta = 27.26$ kg/m^3 isopycnal in the Laurentian Channel plotted on a map. b) Mean ages interpolated to the density of σ_Θ=27.26 kg/m^3 outside the GSL from measurements after 2010. c) SF_6 partial pressure and mean ages in the CIL and the entire deep layer of the Laurentian Channel, with d) zoomed in on around the $\sigma_\Theta = 27.26$ kg/m^3 isopycnal. The red dots display samples measured further east and the blue dots the data from stations westward, with errorbars representing the concentration uncertainty of 2 % (pSF_6 plot), as well as the calculated mean age uncertainty of 10 %. The green line represents the isopycnal of $\sigma_\Theta = 27.26$ kg/m^3 and the red dotted lines the isopycnals of $\sigma_\Theta = 25.25$ kg/m^3 and $\sigma_\Theta = 26.25$ kg/m^3 marking the different water layers. Except for figure b (GLODAP, post 2010 data), all other figures show data collected during the two 2022 TReX cruises within the GSL.

4.3 Water mass analysis

When only considering θ and S_p in the linear least-square water mass fraction analysis, a two-endmember model combing NACW and LCW as described in Section 3.3.1, no presence of LCW on the $\sigma_\Theta = 27.26$ kg/m^3 isopycnal within the Laurentian Channel of the GSL was visible (see Figure S3). This approach solves for the relative fractions of the two source waters based on their characteristic temperature and salinity and showing no presence of LCW occurs because both parameters remain close to the range characteristics of the NACW endmember (see Figure 2), causing the method to attribute all water mass fractions exclusively to NACW. Although the analysis of the individual hydrographic parameters shows along channel variability and indicates the influence of the fresher LCW (see Figure 3), the least-square solution does not capture this.

When considering a third parameter, mean age, in the water mass analysis, which differs significantly between the two source waters, the influence of LCW becomes more pronounced, particularly further inshore (see Figure 5a). Despite inherent uncertainties that limit the interpretation of the estimated fraction values, observational evidence suggests that the fraction of LCW gradually decreases from the west to the east within the Laurentian Channel. The high (up to 100%) LCW fractions near the LSLE reflects uncertainty in the fraction calculations rather than a complete absence of NACW influence.

Applying the 2-IG-TTD approach (see Section 3.3.2) to calculate water mass fractions (mixing factors) yields results consistent with the three-parameter linear fraction analysis (see Figure 5b). The 2-IG-TTD analysis also highlights the increasing influence of LCW inshore, with mixing factors reaching up to ~75% toward the LSLE, compared to ~35% at Cabot Strait, reinforcing the spatial gradient inferred from the linear method.

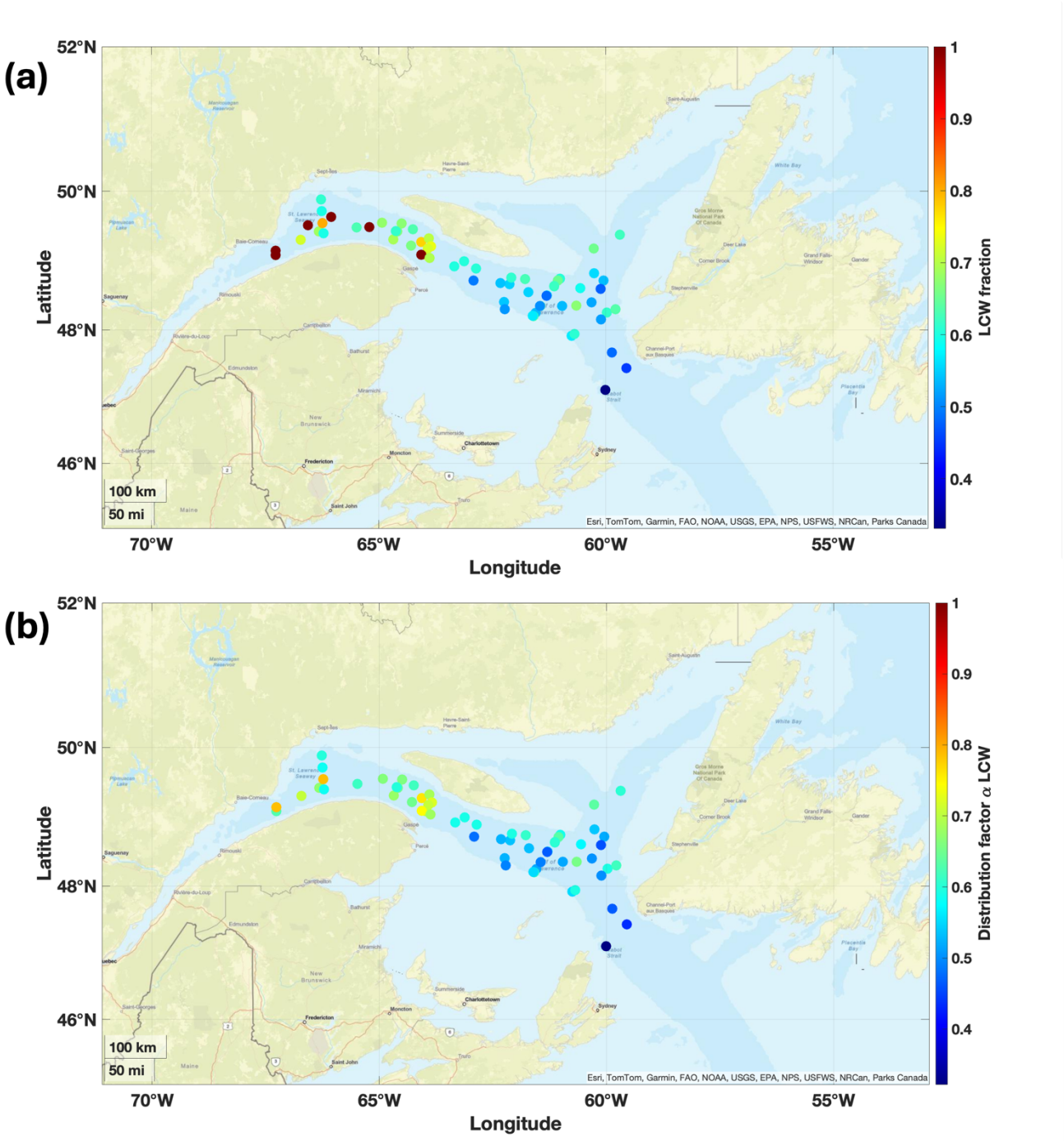

Figure 5: a) LCW fraction on the $\sigma_\Theta = 27.26$ kg/m^3 isopycnal deep water in the Laurentian Channel from θ, S_p and mean age (Γ) observations plotted on a map. The endmembers used in this calculation are provided in Table 1. b) LCW mixing factor on the $\sigma_\Theta = 27.26$ kg/m^3 isopycnal in the Laurentian Channel from the 2-IG-TTD analysis, using observed mean ages (Γ), plotted on a map of the GSL. All the data presented here was collected during the two TReX surveys in 2022.

4.4 Proxy time series at Cabot Strait and full deep water parameter analysis within the Laurentian Channel

The analysis of a proxy time series for mean age and LCW fraction at Cabot Strait from 2018 to 2022 reveals an increase in mean age and decrease in the LCW fraction over time (see Figure 6). Despite these changes, the DO concentrations, when considering the utilization rate within the Laurentian Channel remained relatively stable (see Figure S2) over this four year period, showing only a slight decrease over the time period, although with considerable variability. A linear trend analysis of this decrease indicates that it is not statistically significant, with only 45 datapoints.

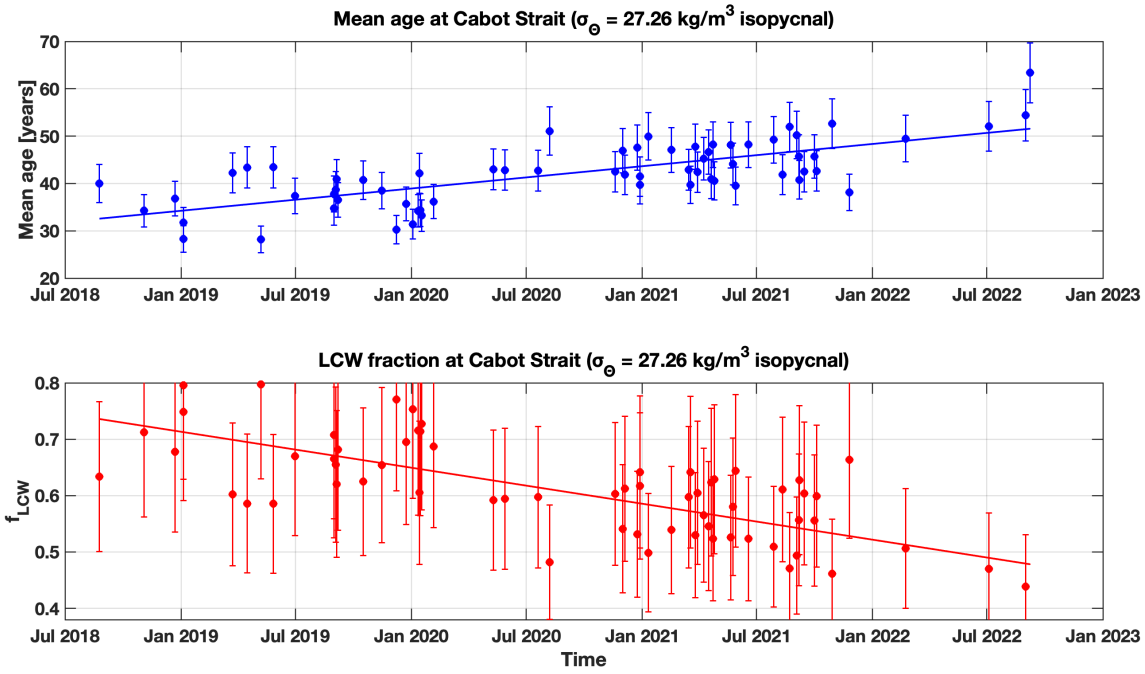

Figure 6: A proxy timeseries of mean age (top) and LCW fraction (bottom) at Cabot Strait from 2018 to 2022. The error bars represent the 10 % uncertainty in the mean age calculation in the upper panel and the 21 % uncertainty from the water mass fraction uncertainty budget in the lower panel. The timeseries data only considers data collected during the two TReX cruises in 2022.

To complement the analysis on the $\sigma_\Theta = 27.26$ kg/m^3 isopycnal within the Laurentian Channel of the GSL, we examined temperature, salinity, mean age and LCW fraction across the full deep water layer (150 to 500 m; $\sigma_\Theta > 26.25$) (see Figure 7). Despite limited data coverage throughout the deep water, this analysis reveals a clear vertical structure. Colder, fresher and younger water dominates in the upper deep layer (toward 150 m) with higher LCW fractions, whereas warmer, saline and older

water is found near the bottom, corresponding to higher NACW fractions. The isopycnals remain relatively flat along the channel, with no shoaling toward the LSLE, which indicates limited vertical mixing. This is consistent with (Stevens et al., 2024), who reported a basin-wide vertical diffusivity of 10^{-5} m^2 s^{-1} over one year in the GSL.

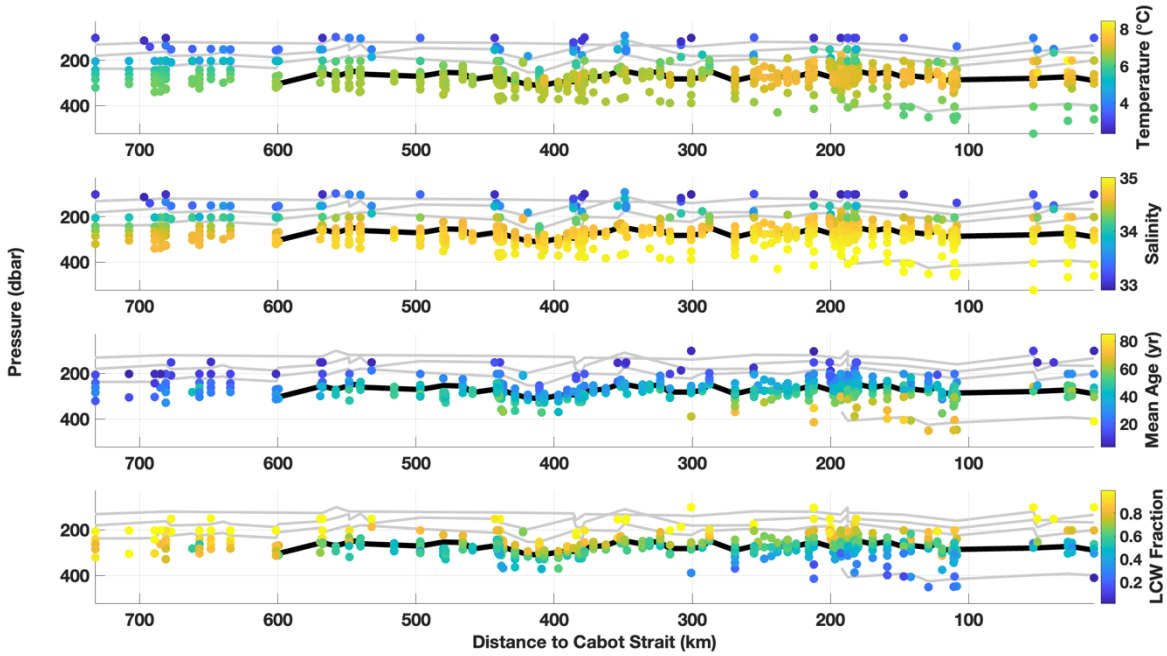

Figure 7: Display of Temperature, Salinity, Mean age and LCW fraction throughout the Laurentian Channel (shown as distance from Cabot Strait, where greater distance corresponds to locations further toward the LSLE) versus depth. The black line indicates the $\sigma_\Theta = 27.26$ kg/m^3 isopycnal and grey lines represent the 26.5, 26.75, 27, and 27.6 isopycnals. (As a reference, the LSLE starts approximately at a distance of 600 km from Cabot Strait)

5 Discussion

The temperature, salinity and mean age analysis of the deep water on the $\sigma_\Theta = 27.26$ kg/m^3 isopycnal along the Laurentian channel show young, cooler, and fresher water in the Lower Estuary and western Gulf, with older, warmer and more saline water entering through Cabot Strait and within the eastern Laurentian Channel (Figures 3, 4a and 7). This pattern appears opposite to what would be expected if the properties evolved along the estuarine circulation pathway along the Laurentian Channel, where water would become progressively older toward the west (Dickie and Trites, 1983). However, this apparent reversal does not imply a change in the estuarine circulation, instead, it might be caused by vertical mixing within the Gulf, e.g. halocline vertical downward motion at intermediate water layers (Galbraith et al., 2024), and/or by changes in the water mass composition of the inflowing deep water. Apart from a rapid shift in all parameters around 63 °W towards older, warmer,

and saltier water in the east, the mean age data shows a gradual age increase from the west to the east (see Figure 4a), consistent with the reconstructed proxy time series at Cabot Strait from 2018 to 2022 (see Figure 6 – upper panel).

The inclusion of transient tracers (SF_6 and CFC-12) in this study enables, for the first time, a direct quantification of ventilation timescales in the Gulf of St. Lawrence, providing new evidence for the temporal evolution and compositional shift of entering deep water.

These observations of water mass ages support the general hypothesis of previous studies suggesting a change in the composition of the Gulf of St. Lawrence's deep inflow towards an increased NACW composition (Galbraith et al., 2024; Jutras et al., 2020). However, recent studies, such as Jutras et al. (2023b), suggest that since 2021 the deep water within the Laurentian Channel has been almost entirely composed of NACW. This finding contrasts with the gradual west to east age increase along the Laurentian Channel observed in this study, suggesting that the influence of NACW on the deep-water composition still continues to increase over time, as of 2022. This highlights that the transition towards NACW dominance is ongoing rather than complete, refining previous assumptions based solely on hydrographic data.

Thus, the observed along-channel gradients in temperature, salinity, and mean age are attributed to the ongoing compositional shift in the inflowing deep waters, rather than to changes in the estuarine circulation.

Supporting this interpretation, our water mass fraction analysis, both incorporating mean age as a tracer with distinctly different source water signatures in the linear fraction model and applying the 2-IG-TTD approach to assess mixing factors, indicates higher LCW fractions near the LSLE, gradually decreasing toward the eastern Gulf (see Figure 5). By combining traditional hydrographic parameters with transient tracer derived mean ages, these approaches provide a more physically constrained assessment of water mass composition and ventilation, offering novel insights beyond previous analysis. This implies that, as of 2022, NACW influence is continuing to rise throughout the Laurentian Channel on the $\sigma_\Theta = 27.26$ kg/m^3 isopycnal from the LSLE to Cabot Strait. Expressed differently, the significant differences in transient tracer concentrations and computed mean ages of the LCW and NACW, provide valuable insight into the evolving water mass composition. While the calculated fraction values itself are subject to significant uncertainty due to model assumptions and endmember variability, the ongoing trend of increasing NACW influence remains identifiable. Despite vertical mixing within the deep water, LCW remains present throughout most of the deep layer in 2022, while pure NACW is only observed near the bottom at Cabot Strait (see Figure 7). No significant shoaling of the studied isopycnal toward the LSLE is evident, indicating that the vertical distribution of water masses is largely maintained along the channel. With the isopycnal measurements on $\sigma_\Theta = 27.26$ kg/m^3 being present at depth of around 300 to 400m along the entire channel, no mixing with intermediate water masses nor even fresher younger surface waters from the St. Lawrence rivers is expected (Jutras et al., 2020). Therefore, the measurements are solely influenced by deep water entering through Cabot Strait.

The LCW and NACW fractions estimated from earlier studies (e.g. Gilbert et al., 2005; Jutras et al., 2020, 2023b) reported ongoing variabilities in the composition of the entering deep water up to a complete disappearance of LCW in 2021. Our observations, however, indicate that this transition is still ongoing as of 2022. In Jutras et al. (2023b), LCW fractions at Cabot Strait were reported as 0 % in 2021, with only a small LCW influence at intermediate depths (~250 m) between the middle of

Anticosti Island to the LSLE. At greater depths they found no LCW influence throughout the Laurentian Channel, in contrast to 2017, when higher LCW fractions were observed closer to the bottom (Jutras et al., 2020).

These recent studies primarily estimate water mass fractions within the Laurentian Channel deep water using basic hydrographic parameters (temperature, salinity, nutrients, oxygen, etc.) combined, for example, with an eOMP analysis, comparable to our simplified water mass analysis approach using temperature and salinity (see Figure S3). The limitation of relying on, e.g., oxygen as an indicator for water mass analysis are evident in our proxy timeseries at Cabot Strait (see Figure S2), where only minor overall changes are detected despite high variability. Moreover, the individual θ and *S*p trends suggest ongoing changes (see Figures 3) and the θ vs. *S*p plot (see Figure 2) shows no overlap with the NACW range, indicating that analysis using only two variables may provide an incomplete picture (Liu and Tanhua, 2021).

The tracer-based framework presented here thus expands the water mass analysis in the GSL by integrating temporal and physical ventilation information through tracer-derived mean ages, a parameter that reflects distinct different source water signatures, providing complementary insights that refine estimates of compositional shifts, offering a more accurate depiction of temporal changes and mixing processes. However, it is important to interpret these results with caution, given uncertainties of up to 21 % in our analysis, as well as the observed intensification of the eastward retroflection of the Labrador Current since 2016 (Jutras et al., 2023a), which has likely contributed to lower LCW fractions than those estimated here.

The lowest LCW fraction and oldest water were observed near Cabot Strait, while higher LCW contributions appeared further west within the Laurentian Channel, indicating that LCW was present throughout the entire Laurentian Channel deep waters in 2022. With regard to oxygen levels, the older water (high NACW fraction) exhibits lower values, as more oxygen has been consumed over time since the water was ventilated from the atmosphere into the interior. In contrast, the younger LCW has only recently been ventilated and thus still carries oxygen-rich water, having just exchanged its oxygen content with atmospheric values. With the oldest water being present at Cabot Strait, this water presumably carries the lowest amount of oxygen. This projection being consistent with findings of Blais et al. (2024), who show a sustained decline in oxygen content at Cabot Strait in 2023 and with the proxy timeseries showing a slight decrease in DO concentrations within the deep water from 2018 to 2022 (see Figure S2). However, this small apparent decrease should be treated with caution, as the time series is statistically insufficient to confirm a significant trend. Given the well-defined age distribution in the Gulf during 2022, future observational and modelling efforts would be valuable to directly link this distribution to DO concentrations and other key biogeochemical parameters. A simplified analysis of the proxy time series, relating mean age and LCW fraction to oxygen concentrations, shows only weak correlations. Despite increasing mean ages and declining LCW fractions from 2018 to 2022, DO levels remained relatively stable, with only a slight decrease. This suggests that variabilities in oxygen concentrations might not be directly tied to water mass changes alone and are likely influenced by additional factors.

A more comprehensive analysis involving multiple biogeochemical parameters is beyond the scope of this current study and would require more consistent tracer surveys to additionally resolve and better capture the effects of short-term (i.e. interannual) inflow variability on the regional age distribution.

As the deep-water flows from Cabot Strait towards the LSLE, the already older water in the eastern part of the Gulf will flow towards the LSLE and further increase the mean age of the deep water in the western part of the Gulf and possibly also increase hypoxia slightly. Given the transit time of around 4.7 years (Stevens et al., 2024) for the bulk of water to travel from Cabot Strait to the LSLE, oxygen levels in the LSLE are expected to continue to drop for the next years on average (Nesbitt et al., 2025).

Over large space and time scales, the observed change in the inflow composition may be linked to a northward shift of the Gulf Stream, which has been suggested in numerous modelling studies (e.g. Claret et al., 2018; Joyce and Zhang, 2010). This northward Gulfstream shift contracts the subpolar gyre and increases the retroflection of LCW, reducing the south-westward transport of LCW towards the mouth of the Laurentian Channel, with implications for the supply of oxygen to the GSL (Jutras et al., 2023a).

6 Conclusions

Transient tracers (SF_6 and CFC-12) were measured for the first time in the GSL to determine ventilation timescales of the deep water on the $\sigma_\Theta = 27.26$ kg/m^3 isopycnal along the Laurentian Channel. These measurements not only provide evidence of an ongoing change in deep water composition as of 2022, but also demonstrate the added value of incorporating transient tracers into water mass analysis.

The observations show a distinct pattern: near the Gulf's entrance, a signal of older, warmer, more saline NACW, while further inshore along the Laurentian Channel, younger, colder, less saline LCW is evident. This along channel gradient contrasts with the expected age pattern based on regional estuarine circulation, which would typically predict older water closer to the LSLE. Instead, it aligns with recent studies suggesting an increasing shift towards older, warmer and saltier NACW over recent years. While previous studies have reported a 100 % NACW contribution present in the deep water in most parts of the Laurentian Channel, as of 2021, using eOMP analysis based solely on hydrographic parameters (Jutras et al., 2023b), our results show that a fraction of LCW is still present throughout the channel, though decreasing from west to east. By including tracer-derived mean ages as a parameter into a water mass analysis, we were able to capture and highlight these ongoing compositional shifts, with a proxy time series further illustrating a temporal decrease in LCW fractions between 2018 and 2022. While the exact fraction values are subject to uncertainties, the broader trend remains evident.

The gradual, ongoing change towards increased NACW fractions may contribute to further reduction of the oxygen content within the GSL, consistent with long-term observations of Blais et al. (2024), who reported decreasing oxygen levels all throughout their time series until 2023. These findings highlight the value of including transient tracers as a parameter in future water mass analysis to more accurately resolve temporal changes, mixing processes, and their associated biogeochemical impacts. Ultimately, the results reflect a, by 2022, continued, ongoing, measurable shift towards greater NACW influence on the GSL entering deep water.

Appendix A: Analysis system

The gas chromatographic – electron capture detector (GC-ECD) system consisted of a precolumn packed with 30 cm Porasil C and 60 cm Molesieve 5A, followed by a main column packed with 200 cm Carbograph 1AC and 20 cm Molsieve 5A. Throughout the measurement, these components were kept at a constant temperature of 50 °C. The function of these columns was to separate the various analytes before concentration determination with the electron capture detector.

Before the analysis, the purge and trap unit extracted the analytes from the water sample by bubbling N_2 gas though the sample and trapping them on a column of 100 cm 1/16" tubing, packed with 70 cm Heysep D. To ensure efficient trapping, this column was kept at -60 to -70 °C using liquid nitrogen and subsequently heated to 100 °C to desorb the analytes onto the precolumn. The water samples were collected in 250 mL glass syringes directly from the Niskin bottles and after temporal storage in a 0 °C water bath, 200 mL of the sample volume was injected into the purge and trap unit.

The system was calibrated by measuring precise volumes of a calibrated gaseous standard containing known analyte concentrations. A calibration curve was recorded at the beginning of each cruise and to determine any drift in the detector, point calibration was carried out daily.

Due to high variations and unusual high concentrations reported during DFO's AZMP Survey/TReX 4, we compared the results to measured samples during TReX 2 at similar density and location. This resulted in a scaling of the CFC-12 measurements by -20 % and SF_6 by -14 % in order to achieve internal consistency between the values (see Figure S4). We conclude that the measured values from TReX 2 are more accurate, as they show tracer concentrations in the surface layer close to 100 % saturation with the atmospheric values of 2022 and in general have less scatter in the data compared to TReX 4. This shift of the November cruise measurements towards plausible and similar values, and only having two datasets throughout the year limits the analysis of any interannual variability, but allows us to perform a Gulf-wide analysis of the age distribution.

Appendix B: Transit time distribution (TTD) analysis

The transit time distribution (TTD) is a well-established concept looking at ventilation timescales via mean age calculation using measured transient tracer concentrations. Thereby, additionally achieving knowledge on the ratio between advective and diffusive transport of water masses from the surface into the interior ocean (e.g. Stöven and Tanhua, 2014; Waugh et al., 2003). TTD determination is possible using a tracer couple sampled at the same location and time with significant different input functions, as being the case for SF_6 and CFC-12 during the two cruises analyzed in this study.

The method is based on a function describing the concentration of a single tracer at a certain location ($c(t_s,r)$), calculated using boundary concentrations of this tracer, related to their input function, and Green's function (G(t,r)) (see Equation 5).

$$c(t_s, r) = \int_0^\infty c_0(t_s - t)e^{-\lambda t} \times G(t, r)dt \quad (5)$$

Applying four assumptions, being (1) a steady state, (2) a single source region, (3) no inner water interactions affecting the concentration of the tracer and (4) a one-dimensional flow, and assuming an inverse Gaussian (IG) age distribution, the Inverse Gaussian Transit Time Distribution (IG-TTD) provides one solution for the TTD. Considering distinct sampling points of a tracer, Green's function (G(t)) at a particular time can be characterized by the mean age (Γ) and the width of the distribution (Δ), excluding the location (see Equation 6) (Schneider et al., 2012; Sonnerup et al., 2013; Stöven and Tanhua, 2014; Waugh et al., 2002).

$$G(t) = \sqrt{\frac{\Gamma^3}{4\pi\Delta^2 t^3}} \times \exp\left(\frac{-\Gamma(t-\Gamma)^2}{4\Delta^2 t}\right) \quad (6)$$

The ratio of width to mean age (Δ/Γ), describes the above-mentioned relationship of advective to diffusive flow. A Δ/Γ-ratio of 1.0 is the unity ratio, Δ/Γ-ratio > 1 indicate a diffusive dominating process and a Δ/Γ-ratio < 1 a more advective ventilation of a water parcel.

The initial attempt to constrain the TTD in this study and gain information on the Δ/Γ-ratio involved a standard approach of comparing mean ages derived from CFC-12 to SF_6 measurements at the same location and time (see Figure B1a). This method compares the mean ages derived from the individual tracers under varying Δ/Γ-ratios. Agreement between the two tracer-derived mean ages (yellow lines in Figure B1a) indicates that the chosen Δ/Γ-ratio would reflect local advective and diffusive transport characteristics well. However, this method did not yield sufficient results across all ratios, as in all cases the CFC-12 based mean ages were generally higher than those derived from SF_6 (optimal outcomes would align the data points on top or close to the 1:1 line). One potential reason for this discrepancy could be the assumption of a steady state in ventilation, which is not the case in the Gulf (see main part of the paper). Additionally, uncertainties may arise from the assumed inverse Gaussian shape of the TTD, which might not be practical to use in this area and/or from the presence of only rather young waters, affecting the calculations from CFC-12 measurements, given the tracers atmospheric history of declining concentrations since 2002 (see Figure S1).

To test this last hypothesis, we compared measured and calculated CFC-12 concentrations (again under varying Δ/Γ-ratios) relative to observed SF_6 concentrations measured at the same location and time. We derived mean ages from SF_6 concentrations and back calculated the corresponding CFC-12 concentrations, which were then compared to the actual measured concentrations. Figure B1b, S5 and S6 show the difference between expected to measured CFC-12 concentrations as a function of the SF_6 partial pressures for varying Δ/Γ-ratios. The calculated values were consistently slightly higher than the measured values (above the blue line representing a perfect match of calculated and measured CFC-12) across the full range of SF_6 concentrations (2-8 ppt), with no systematic trend towards higher SF_6 values representing recently ventilated waters. We therefore conclude that the influence of decreasing pCFC-12 in the atmosphere is not a relevant factor for our TTD analysis in

545 this region. The difficulty in constraining the TTD thus mainly arises from the assumptions made for the calculation, being the steady state, the single source region and the inverse Gaussian shape.

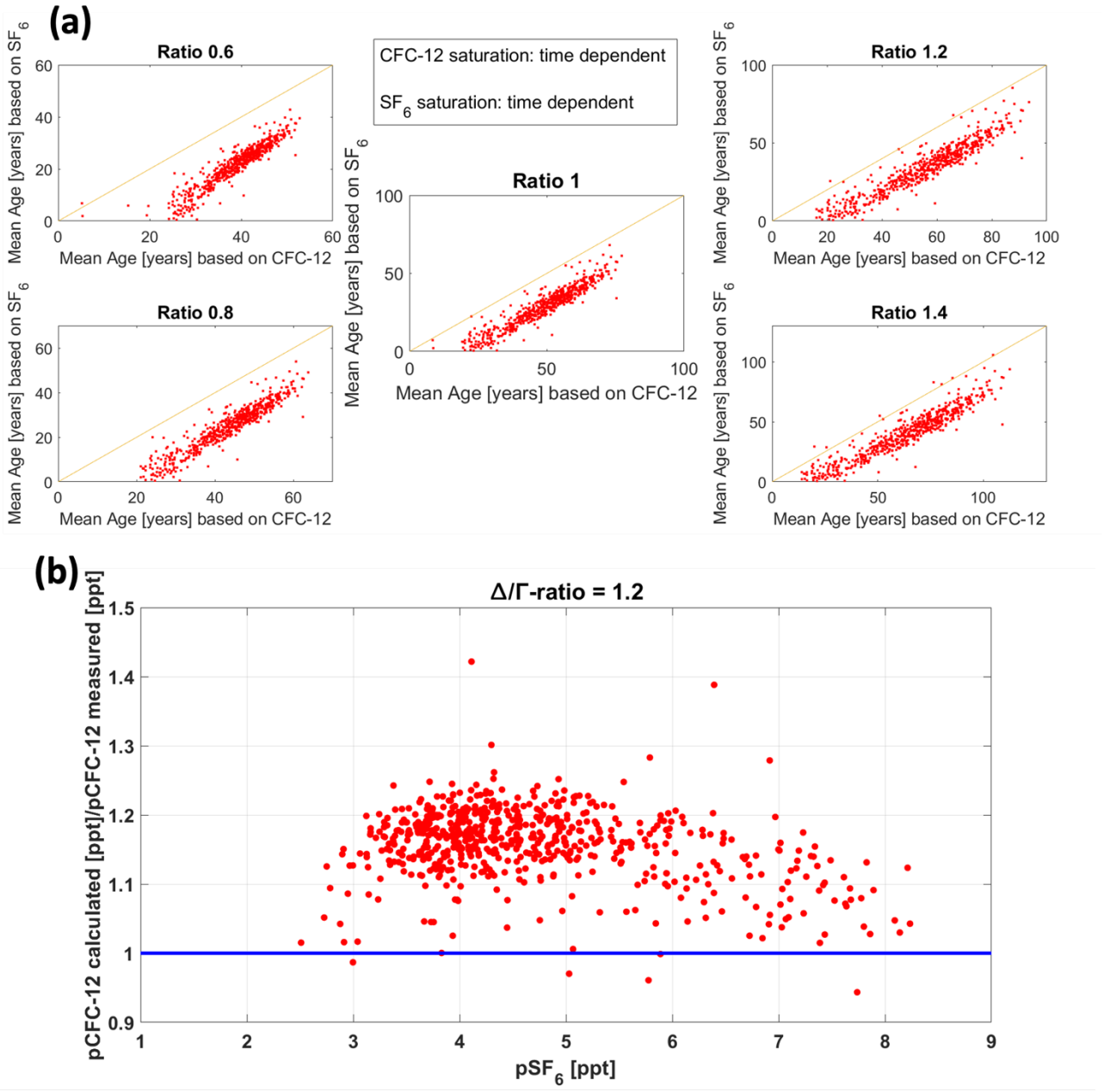

Figure B1: a) Comparison of calculated mean ages from CFC-12 and SF_6 with different Δ/Γ-ratio. The saturations for each tracer 550 **were assumed to be time dependent. b) Display of the relationship between calculated and measured pCFC-12 against pSF_6 concentrations using a ratio of Δ/Γ=1.2 for the calculations.**

Both methods applied indicate the best results with increasing Δ/Γ-ratio, either by mean ages converging toward the 1:1 yellow line (method 1) or by calculated to measured concentration ratios approaching unity (method 2), suggesting a diffusive dominated transport. The most suitable result from these analysis is obtained with a Δ/Γ-ratio of > 1.8, indicated by datapoints being closest to the yellow and blue lines. However, Stöven et al. (2015) concluded that with increasing ratios Δ/Γ-ratios, the calculated mean ages become more sensitive to deviations in saturation and tracer age. Consequently, we selected a Δ/Γ-ratio of 1.2 as an optimal balance, along with the time dependent saturation analyzed by Raimondi et al. (2021) in the Labrador Sea, for the calculation of mean ages in this study. This choice reflects a slightly diffusive dominated transport (Δ/Γ-ratio > 1) while avoiding excessive age deviations (Δ/Γ-ratio > 1,6).

To further assess the plausibility of our chosen ratio, we examined Δ/Γ results derived from a one-dimensional Gaussian pipe model describing the spreading of the CF_3SF_5 tracer analyzed in Stevens et al. (2024). In this model, Δ/Γ is calculated from the advective ($\Delta=ut$) and diffusive ($\Gamma=(2kt)^{-1/2}$) terms, yielding values of 1.2 and 1.5 for the two surveys (TReX 2 and DFO's AZMP Survey/TReX 4), respectively. These values fall within the same range as the ratio applied in this study, thus providing additional support for our choice.

For the data inside the Gulf of St. Lawrence we primarily focus on the mean ages calculated from SF_6 concentrations due to rather young waters, but for the data outside the Gulf we also include data from CFC-12 concentrations due to the larger quantity of available measurements.

Appendix C: Uncertainty estimates for mean age determination

The uncertainty in the derived mean ages arises from several factors: measurement errors in the transient tracer concentrations, uncertainties in constraining the TTD using various assumptions, and uncertainties in the input function, including atmospheric concentrations and saturation levels. The uncertainty in the transient tracer concentration involves analytical measurement errors, calibration biases (≈ 1 %), and errors arising from the use of a fixed purge efficiency in the calibration (for CFC-12: ≈ 2 %) (Stöven and Tanhua, 2014).

The uncertainty increases when using these tracer concentrations to determine ventilation dynamics and calculating mean ages. Consistent with previous studies, we estimate that the input function contributes a bias to the calculations with 5-10 % (DeGrandpre et al., 2006; Haine and Richards, 1995; Stöven and Tanhua, 2014; Tanhua et al., 2008). This primarily involves the use of a fixed saturation, here the time dependent saturation from the Labrador Sea (Raimondi et al., 2021), as this varies especially at higher latitudes. Additionally, it includes the assumption of non-linearity in tracer solubility, which is influenced by mixing of different water masses in different ways. A minor contribution to the error caused by the input function is using a mean atmospheric concentration derived from measurements at various facilities in the northern hemisphere (Walker et al., 2000). Although this only introduces a bias of less than 1 %.

The assumptions applied to constrain the TTD, such as steady state conditions, a single source region, no inner water interaction, and an inverse Gaussian shape of the distribution, add another source of uncertainty to the calculation of mean ages. The actual distribution may deviate, particularly due to the mixing of various water masses with different time histories, as seen in the merging of the NACW and LCW. Another source of uncertainty arises from the choice of a specific Δ/Γ-ratio, which determines the balance between advective and diffusive flows.

Overall, the combined error, which includes uncertainties from the use of a fixed input function and measurement inaccuracies (the largest contributors), results in an uncertainty of up to 10 %. This error is included in the mean age results in this study. Another uncertainty arises from the application of the uniform Δ/Γ-ratio (1.2) to regions outside the Gulf of St. Lawrence (NACW and LCW), where only CFC-12 measurements were available. This limitation prevents direct determination of local Δ/Γ values from tracer pairs and may introduce biases when applying a fixed ratio, as discussed by Guo et al. (2025).

Appendix D: Uncertainty budget for water mass fraction analysis

To account for uncertainties in the water mass fraction analysis, we developed a detailed uncertainty budget that explicitly incorporates individual sources of uncertainty. All sources were simultaneously propagated using a Monte Carlo simulation with 10,000 realizations.

The first source of uncertainty comes from the choice of the endmembers for each parameter, including mean age, temperature and salinity. The mean age endmembers were determined by calculating the mean of all measurements since 2010 for each water mass in the Atlantic Ocean. Therefore, the associated error was computed as the standard error of the mean (SEM), as follows:

- **NACW**
  a. Endmember range of all included measurements: 49-105 years
  b. Mean of all included measurements: 86.5 years
  c. Standard deviation: $\sigma_{\Gamma,NACW} = 13.16$
  d. $$Standard\ error\ of\ the\ mean\ (SEM) = \frac{\sigma_{\Gamma,NACW}}{\sqrt{number\ of\ included\ samples}} = 1.67\ years \quad (7)$$
  e. $$Relative\ SEM = \frac{1.67\ years}{86.5\ years} = 1.93\% \quad (8)$$

- **LCW**
  a. Endmember range of all included measurements: 7-19 years
  b. Mean of all included measurements: 12.5 years
  c. Standard deviation: $\sigma_{\Gamma,LCW} = 3.29$
  d. $$Standard\ error\ of\ the\ mean\ (SEM) = \frac{\sigma_{\Gamma,LCW}}{\sqrt{number\ of\ included\ samples}} = 0.23\ years \quad (9)$$
  e. $$Relative\ SEM = \frac{0.23\ years}{86.5\ years} = 1.84\% \quad (10)$$

For salinity and temperature endmembers, the range for each water mass were taken from Jutras et al. (2020), and the uncertainty were derived as the standard deviation of a uniform distribution over these range (see Equations 11 through 14):

- **NACW temperature**
  a. Endmember range: 4.4 °C – 8 °C (±0.2 °C)
  b. Middle of range: 6.2 °C (±0.2 °C)
  c. Standard deviation of uniform distribution: $\sigma_{\Theta,NACW} = \frac{(8\,°C - 4.4\,°C)}{\sqrt{12}} = \frac{3.6\,°C}{\sqrt{12}} = 1.04°C$ (11)

- **LCW temperature**
  a. Endmember range: -0.7 °C – 3.2 °C (±0.2 °C)
  b. Middle of range: 1.25 °C (±0.2 °C)
  c. Standard deviation of uniform distribution: $\sigma_{\Theta,LCW} = \frac{(3.2\,°C - (-0.7\,°C))}{\sqrt{12}} = \frac{3.9\,°C}{\sqrt{12}} = 1.13°C$ (12)

- **NACW salinity**
  a. Endmember range: 35 psu – 35.2 psu (±1.2 psu)
  b. Middle of range: 35.1 psu (±1.2 psu)
  c. Standard deviation of uniform distribution: $\sigma_{Sp,NACW} = \frac{(35.2\,psu - 35\,psu)}{\sqrt{12}} = \frac{0.2\,psu}{\sqrt{12}} = 0.06\,psu$ (13)

- **LCW salinity**
  a. Endmember range: 33.4 psu – 35 psu (±0.5 psu)
  b. Middle of range: 34.2 psu (±0.5 psu)
  c. Standard deviation of uniform distribution: $\sigma_{Sp,LCW} = \frac{(35\,psu - 33.4\,psu)}{\sqrt{12}} = \frac{1.6\,psu}{\sqrt{12}} = 0.46\,psu$ (14)

Furthermore, the mean ages observed within the GSL and used in the fraction analysis were assigned a relative uncertainty of 10 % (see Appendix C). To account for model simplifications associated with using a simple linear mixing model and a least square solution, an additional 20 % relative uncertainty was included.

All uncertainties were then jointly propagated using a Monte Carlo simulation with 10,000 realizations (JCGM, 2008), resulting in a final relative uncertainty of approximately 21 % for the estimated LCW fractions.

Data availability:

The transient tracer and CTD data of the two cruises analyzed in this study will be made available through the open research repository 'Canadian Integrated Ocean Observing System – St. Lawrence Global Observatory' (CIOOS-SLGO) via https://doi.org/10.26071/d6f3fdfc-788d-48ff. These datasets are part of an integrated data product documenting a 20-year

biogeochemical time series in the Gulf of St. Lawrence region. The metadata is already publicly accessible, while the data itself will be released following the submission of a related data manuscript. Additionally, the CTD data from the DFO AZMP survey can be requested at https://open.canada.ca/en.

Historical transient tracer data used from the GLODAPv2.2022 data product can be found at https://www.ncei.noaa.gov/access/ocean-carbon-acidification-data-system/oceans/GLODAPv2_2022/.

Author contribution:

LG, WAN, SWS and TT conceived the study. LG, WAN, SWS and DWRW coordinated and conducted at-sea campaigns. LG conducted analysis and wrote the manuscript with writing and editorial contributions from all authors.

Competing interests:

The authors declare that they have no conflict of interest.

Acknowledgments:

We are grateful to REFORMAR and the captains and crew of the *R/V Coriolis II* for support on the cruises. We want to thank the National Research Council's Oceans program and the Department of Fisheries and Oceans for providing additional ship time support for the TReX Deep experiment. Specifically, thanks to Dr. Marjolaine Blais for allowing us to participate on the 2022 AZMP cruise and for sharing the data. Finally, we would also like to acknowledge other researchers on board for their support, especially Adriana Reitano, Marshal Thrasher, and Jeshua Becker, and all scientists and technicians who contributed to the data in GLODAPv2.2022.

Financial support:

Financial support for the TReX project was provided by the Marine Environmental Observation, Prediction and Response (MEOPAR) Network of Centres of Excellence and the Réseau Québec maritime and its Odyssée Saint-Laurent ship time program. Partial support for student personnel and technical assistance was provided by a NSERC Discovery Grant to DWRW. SWS's participation was supported by a TReX Graduate Award, a UBC Four-Year fellowship, and a postdoctoral fellowship from the Tula Foundation.

References

Azetsu-Scott, K., Jones, E. P., and Gershey, R. M.: Distribution and ventilation of water masses in the Labrador Sea inferred from CFCs and carbon tetrachloride, Mar Chem, 94, 55–66, https://doi.org/10.1016/j.marchem.2004.07.015, 2005.

Blais, M., Galbraith, P. S., Plourde, S., and Fisheries, C. L.: Chemical and Biological Oceanographic Conditions in the Estuary and Gulf of St. Lawrence during 2022, Can. Tech. Rep. Hydrogr. Ocean Sci., 357, v-70p, 2023.

Blais, M., Galbraith, P. S., Lizotte, M., Clay, S. A., and Starr, M.: Chemical and Biological Oceanographic Conditions in the Estuary and Gulf of St. Lawrence During 2023, Can. Tech. Rep. Hydrogr. Ocean Sci., 385, v-84p, 2024.

Bugden, G. L.: Oceanographic conditions in the deeper waters of the Gulf of St. Lawrence in relation to local and oceanic forcing, NAFO Scientific Council Studies documents, 88, 87, 1988.

Bullister, J. L. and Warner, M. J.: Atmospheric Histories (1765-2022) for CFC-11, CFC-12, CFC-113, CCl4, SF6 and N2O (NCEI Accession 0164584). [CFC-12, SF6], 2017.

Bullister, J. L., Wisegarver, D. P., and Menzia, F. A.: The solubility of sulfur hexafluoride in water and seawater, Deep Sea Research Part I: Oceanographic Research Papers, 49, 175–187, https://doi.org/10.1016/S0967-0637(01)00051-6, 2002.

Claret, M., Galbraith, E. D., Palter, J. B., Bianchi, D., Fennel, K., Gilbert, D., and Dunne, J. P.: Rapid coastal deoxygenation due to ocean circulation shift in the northwest Atlantic, https://doi.org/10.1038/s41558-018-0263-1, 1 October 2018.

DeGrandpre, M. D., Körtzinger, A., Send, U., Wallace, D. W. R., and Bellerby, R. G. J.: Uptake and sequestration of atmospheric CO2 in the Labrador Sea deep convection region, Geophys Res Lett, 33, https://doi.org/10.1029/2006GL026881, 2006.

Diaz, R. J. and Rosenberg, R.: Spreading Dead Zones and Consequences for Marine Ecosystems, Science (1979), 321, 926–929, https://doi.org/10.1126/science.1156401, 2008.

Dickie, L. and Trites, R.: The Gulf of St. Lawrence, in: Ecosystems of the World: Estuaries and enclosed seas, edited by: Ketchum, B., Elsevier, New York, NY, 1983.

Fennel, K. and Testa, J. M.: Biogeochemical Controls on Coastal Hypoxia, Annu. Rev. Mar. Sci, 11, 105–130, https://doi.org/10.1146/annurev-marine-010318, 2019.

Fine, R. A.: Observations of CFCs and SF 6 as ocean tracers, Ann Rev Mar Sci, 3, 173–195, https://doi.org/10.1146/annurev.marine.010908.163933, 2011.

Galbraith, P. S.: Winter water masses in the Gulf of St. Lawrence, Journal of Geophysical Research: Atmospheres, 111, https://doi.org/10.1029/2005JC003159, 2006.

Galbraith, P. S., Chassé, J., Shaw, J.-L., Dumas, J., and Bourassa, M.-N.: Physical Oceanographic Conditions in the Gulf of St. Lawrence during 2023, Can. Tech. Rep. Hydrogr. Ocean Sci., 378, v-91p, 2024.

Genovesi, L., de Vernal, A., Thibodeau, B., Hillaire-Marcel, C., Mucci, A., and Gilbert, D.: Recent changes in bottom water oxygenation and temperature in the gulf of st. Lawrence: Micropaleontological and geochemical evidence, Limnol Oceanogr, 56, 1319–1329, https://doi.org/10.4319/lo.2011.56.4.1319, 2011.

Gerke, L., Arck, Y., and Tanhua, T.: Temporal Variability of Ventilation in the Eurasian Arctic Ocean, J Geophys Res Oceans, 129, https://doi.org/10.1029/2023JC020608, 2024.

Gilbert, D.: Propagation of temperature signals from the northwest Atlantic continental shelf edge into the Laurentian Channel, ICES CM, 2004, 12p, 2004.

Gilbert, D. and Pettigrew, B.: Interannual variability (1948-1994) of the CIL core temperature in the Gulf of St. Lawrence, Can. J. Fish. Aquat. Sci, 54, 57–67, 1997.

Gilbert, D., Sundby, B., Gobeil, C., Mucci, A., and Tremblay, G. H.: A seventy-two-year record of diminishing deep-water oxygen in the St. Lawrence estuary: The northwest Atlantic connection, Limnol Oceanogr, 50, 1654–1666, https://doi.org/10.4319/lo.2005.50.5.1654, 2005.

Grantham, B. A., Chan, F., Nielsen, K. J., Fox, D. S., Barth, J. A., Huyer, A., Lubchenco, J., and Menge, B. A.: Upwelling-driven nearshore hypoxia signals ecosystem and oceanographic changes in the northeast Pacific, Nature, 429, 749–754, https://doi.org/10.1038/nature02605, 2004.

Guo, H., Koeve, W., Oschlies, A., He, Y.-C., Kemena, T. P., Gerke, L., and Kriest, I.: Dual-tracer constraints on the inverse Gaussian transit time distribution improve the estimation of water mass ages and their temporal trends in the tropical thermocline, Ocean Science, 21, 1167–1182, https://doi.org/10.5194/os-21-1167-2025, 2025.

Haine, T. W. N. and Richards, K. J.: Haine et al. 1995, J Geophys Res, 100, 10,727-10,744, 1995.

Hall, T. M. and Plumb, R. A.: Age as a diagnostic of stratospheric transport, Journal of Geophysical Research: Atmospheres, 99, 1059–1070, 1994.

Hansen, H. P.: Determination of oxygen, in: Methods of Seawater Analysis, Wiley, 75–89, https://doi.org/10.1002/9783527613984.ch4, 1999.

Joint Committee for Guides in Metrology (JCGM): Evaluation of measurement data-Supplement 1 to the "Guide to the expression of uncertainty in measurement"-Propagation of distributions using a Monte Carlo method., 2008.

Joyce, T. M. and Zhang, R.: Notes and correspondence: On the Path of the Gulf Stream and the Atlantic meridional overturning circulation, J Clim, 23, 3146–3154, https://doi.org/10.1175/2010JCLI3310.1, 2010.

Jutras, M., Dufour, C. O., Mucci, A., Cyr, F., and Gilbert, D.: Temporal Changes in the Causes of the Observed Oxygen Decline in the St. Lawrence Estuary, J Geophys Res Oceans, 125, https://doi.org/10.1029/2020JC016577, 2020.

Jutras, M., Dufour, C. O., Mucci, A., and Talbot, L. C.: Large-scale control of the retroflection of the Labrador Current, Nat Commun, 14, https://doi.org/10.1038/s41467-023-38321-y, 2023a.

Jutras, M., Mucci, A., Chaillou, G., Nesbitt, W. A., and Wallace, D. W. R.: Temporal and spatial evolution of bottom-water hypoxia in the St Lawrence estuarine system, Biogeosciences, 20, 839–849, https://doi.org/10.5194/bg-20-839-2023, 2023b.

Khatiwala, S., Visbeck, M., and Schlosser, P.: Age tracers in an ocean GCM, Deep-Sea Research I, 48, 1423–1441, 2001.

Koutitonsky, V. G. and Budgen, G. L.: The physical oceanography of the Gulf of St. Lawrence : a review with emphasis on the synoptic variability of the motion, Can. Spec. Publ. Fish. Aquat. Sci., 113, 57–90, 1991.

Lauvset, S. L. and et al.: GLODAPv2. 2022: the latest version of the global interior ocean biogeochemical data product, Earth Syst Sci Data, 14, 5543–5572, https://doi.org/10.5194/essd-14-5543-2022, 2022.

Lauzier, L. M. and Trites, R. W.: The Deep Waters in the Laurentian Channel, Journal of the Fisheries Research Board of Canada, 15, 1247–1257, https://doi.org/10.1139/f58-068, 1958.

Lehmann, M. F., Barnett, B., Geĺinas, Y., Gilbert, D., Maranger, R. J., Mucci, A., Sundby, B., and Thibodeau, B.: Aerobic respiration and hypoxia in the lower st. lawrence estuary: Stable isotope ratios of dissolved oxygen constrain oxygen sink partitioning, Limnol Oceanogr, 54, 2157–2169, https://doi.org/10.4319/lo.2009.54.6.2157, 2009.

Liu, M. and Tanhua, T.: Water masses in the Atlantic Ocean: Characteristics and distributions, Ocean Science, 17, 463–486, https://doi.org/10.5194/os-17-463-2021, 2021.

McLellan, H. J.: On the Distinctness and Origin of the Slope Water off the Scotian Shelf and its Easterly Flow South of the Grand Banks, Journal of the Fisheries Research Board of Canada, 14, 213–239, https://doi.org/10.1139/f57-011, 1957.

Mucci, A., Starr, M., Gilbert, D., and Sundby, B.: Acidification of Lower St. Lawrence estuary bottom waters, Atmosphere - Ocean, 49, 206–218, https://doi.org/10.1080/07055900.2011.599265, 2011.

Nesbitt, W. A., Stevens, S. W., Mucci, A. O., Gerke, L., Tanhua, T., Chaillou, G., and Wallace, D. W. R.: The coupled oxygen and carbon dynamics in the subsurface waters of the Gulf and Lower St. Lawrence Estuary and implications for artificial oxygenation, Ocean Science, 21, 2179–2195, https://doi.org/10.5194/os-21-2179-2025, 2025.

Raimondi, L., Tanhua, T., Azetsu-Scott, K., Yashayaev, I., and Wallace, D. W. R.: A 30 -Year Time Series of Transient Tracer-Based Estimates of Anthropogenic Carbon in the Central Labrador Sea, J Geophys Res Oceans, 126, https://doi.org/10.1029/2020JC017092, 2021.

Rousseau, S., Lavoie, D., Jutras, M., and Chassé, J.: Transit time of deep and intermediate waters in the Gulf of St. Lawrence, Ocean Model (Oxf), 195, https://doi.org/10.1016/j.ocemod.2025.102526, 2025.

Saucier, F. J., Roy, F., Gilbert, D., Pellerin, P., and Ritchie, H.: Modeling the formation and circulation processes of water masses and sea ice in the Gulf of St. Lawrence, Canada, J Geophys Res Oceans, 108, https://doi.org/10.1029/2000jc000686, 2003.

Schneider, A., Tanhua, T., Körtzinger, A., and Wallace, D. W. R.: An evaluation of tracer fields and anthropogenic carbon in the equatorial and the tropical North Atlantic, Deep Sea Res 1 Oceanogr Res Pap, 67, 85–97, https://doi.org/10.1016/j.dsr.2012.05.007, 2012.

Shao, A. E., Mecking, S., Thompson, L. A., and Sonnerup, R. E.: Evaluating the use of 1-D transit time distributions to infer the mean state and variability of oceanic ventilation, J Geophys Res Oceans, 121, 6650–6670, https://doi.org/10.1002/2016JC011900, 2016.

Shaw, J. L. and Galbraith, P. S.: Climatology of Transport in the Strait of Belle Isle, J Geophys Res Oceans, 128, https://doi.org/10.1029/2022JC019084, 2023.

Sonnerup, R. E., Mecking, S., and Bullister, J. L.: Transit time distributions and oxygen utilization rates in the Northeast Pacific Ocean from chlorofluorocarbons and sulfur hexafluoride, Deep Sea Research Part I: Oceanographic Research Papers, 72, 61–71, https://doi.org/10.1016/j.dsr.2012.10.013, 2013.

Stevens, S. W., Pawlowicz, R., Tanhua, T., Gerke, L., Nesbitt, W. A., Drozdowski, A., Chassé, J., and Wallace, D. W. R.: Deep inflow transport and dispersion in the Gulf of St. Lawrence revealed by a tracer release experiment, Commun Earth Environ, 5, 1–13, https://doi.org/10.1038/s43247-024-01505-5, 2024.

Stöven, T. and Tanhua, T.: Ventilation of the mediterranean sea constrained by multiple transient tracer measurements, Ocean Science, 10, 439–457, https://doi.org/10.5194/os-10-439-2014, 2014.

Stöven, T., Tanhua, T., Hoppema, M., and Bullister, J. L.: Perspectives of transient tracer applications and limiting cases, Ocean Science, 11, 699–718, https://doi.org/10.5194/os-11-699-2015, 2015.

Talley, L. D., Feely, R. A., Sloyan, B. M., Wanninkhof, R., Baringer, M. O., Bullister, J. L., Carlson, C. A., Doney, S. C., Fine, R. A., Firing, E., Gruber, N., Hansell, D. A., Ishii, M., Johnson, G. C., Katsumata, K., Key, R. M., Kramp, M., Langdon, C., Macdonald, A. M., Mathis, J. T., McDonagh, E. L., Mecking, S., Millero, F. J., Mordy, C. W., Nakano, T., Sabine, C. L., Smethie, W. M., Swift, J. H., Tanhua, T., Thurnherr, A. M., Warner, M. J., and Zhang, J.-Z.: Changes in Ocean Heat, Carbon Content, and Ventilation: A Review of the First Decade of GO-SHIP Global Repeat Hydrography, Ann Rev Mar Sci, 8, 185–215, https://doi.org/10.1146/annurev-marine-052915-100829, 2016.

Tanhua, T., Anders Olsson, K., and Fogelqvist, E.: A first study of SF 6 as a transient tracer in the Southern Ocean, Deep Sea Res 2 Top Stud Oceanogr, 51, 2683–2699, https://doi.org/10.1016/j.dsr2.2001.02.001, 2004.

Tanhua, T., Olsson, K. A., and Jeansson, E.: Formation of Denmark Strait overflow water and its hydro-chemical composition, Journal of Marine Systems, 57, 264–288, https://doi.org/10.1016/j.jmarsys.2005.05.003, 2005a.

Tanhua, T., Bulsiewicz, K., and Rhein, M.: Spreading of overflow water from the Greenland to the Labrador Sea, Geophys Res Lett, 32, 1–4, https://doi.org/10.1029/2005GL022700, 2005b.

Tanhua, T., Waugh, D. W., and Wallace, D. W. R.: Use of SF6 to estimate anthropogenic CO2 in the upper ocean, J Geophys Res Oceans, 113, https://doi.org/10.1029/2007JC004416, 2008.

Thibodeau, B., de Vernal, A., and Mucci, A.: Recent eutrophication and consequent hypoxia in the bottom waters of the Lower St. Lawrence Estuary: Micropaleontological and geochemical evidence, Mar Geol, 231, 37–50, https://doi.org/10.1016/j.margeo.2006.05.010, 2006.

Trossman, D. S., Thompson, L., Mecking, S., and Warner, M. J.: On the formation, ventilation, and erosion of mode waters in the North Atlantic and Southern Oceans, J Geophys Res Oceans, 117, https://doi.org/10.1029/2012JC008090, 2012.

Walker, S. J., Weiss, R. F., and Salameh, P. K.: Reconstructed histories of the annual mean atmospheric mole fractions for the halocarbons CFC-11, CFC-12, CFC-113, and carbon tetrachloride, J Geophys Res Oceans, 105, 14285–14296, https://doi.org/10.1029/1999jc900273, 2000.

Warner, M. J. and Weiss, R. F.: Solubilities of chlorofluorocarbons 11 and 12 in water and seawater, Deep Sea Research Part A. Oceanographic Research Papers, 32, 1485–1497, https://doi.org/https://doi.org/10.1016/0198-0149(85)90099-8, 1985.

Waugh, D. W., Vollmer, M. K., Weiss, R. F., Haine, T. W. N., and Hall, T. M.: Transit time distributions in Lake Issyk-Kul, Geophys Res Lett, 29, https://doi.org/10.1029/2002gl016201, 2002.

Waugh, D. W., Hall, T. M., and Haine, T. W. N.: Relationships among tracer ages, J Geophys Res, 108, https://doi.org/10.1029/2002jc001325, 2003.